Evaluation of dose calculations and couch positional accuracy in the context of dynamic couch trajectories

Joel Mullins

Master of Science

Medical Physics Unit

McGill University

Montreal, QC

2013-12-15

A thesis submitted to McGill University in partial fulfillment of the requirements of the degree of Masters of Science, Medical Radiation Physics

ACKNOWLEDGEMENTS

Several people have aided me in my research and preparation of this thesis. I would like to thank my supervisors, Alasdair Syme and Jan Seuntjens, for their help and advice along the way, as well as the editing of this thesis. Thank you to Michael Fan for our discussions on research. Thank you to Marc-André Renaud for assisting in the translation of the abstract. Finally, thank you to my parents for their encouragement and unwavering support.

ABSTRACT

The Varian TrueBeam STx linear accelerator features a developer's mode in which treatment plans can be programmed that include patient couch motion during radiation delivery. The combination of synchronous couch/gantry trajectories with Varian volumetric modulated arc therapy (VMAT) optimizations, called RapidArc, can result in a treatment technique that has been designated Virtual Isocenter RapidArc (VIRA). Prior to its implementation, the accuracy of dose calculations in the Varian Eclipse treatment planning system, on which the RapidArc optimization depends, must be validated, as well as the positional accuracy of the TrueBeam patient couch. The dose calculation accuracy was evaluated extrinsically through the delivery of clinical dynamic multileaf collimator (DMLC) intensity modulated radiotherapy (IMRT) treatment plans as a function of source-to-surface distance (SSD) and measurement with ionization chamber and Gafchromic EBT3 film. Parameters intrinsic to dose calculations in Eclipse, the dosimetric leaf gap (DLG) and leaf transmission (LT), were also investigated for their dependence on SSD. The positional accuracy of the treatment couch was assessed through the generation of treatment plans with static couch/gantry, static couch/rotating gantry, and synchronous couch and gantry motion, with measurement of the real-time ionization chamber current positioned in a cylindrical phantom during radiation delivery. The relative agreement of ionization chamber measurements to Eclipse dose calculations for DMLC IMRT treatment plans decreased by 1.5±0.3% over SSDs in the range of 85 cm to 135 cm (less than 1.0% deviation from standard clinical reference conditions of 100 cm SSD). Gafchromic

EBT3 film measurements were consistent with ionization chamber results, though noise in the film data at low doses resulted in large uncertainties. Measurements of DLG were independent of SSD, following corrections for geometric projection. LT showed a dependence on SSD of 0.09±0.02% over the SSD range investigated. The ionization chamber current measurements for synchronous couch and gantry rotation, analogous to the proposed VIRA technique, indicated a maximum deviation of 0.2 cm relative to treatment isocenter, equal to the deviation observed for the rotating gantry/static couch treatment, analogous to conventional VMAT delivery. These results indicate that the Varian TrueBeam and Eclipse maintain the necessary positional and dosimetric accuracy required for VMAT treatments involving dynamic couch trajectories.

ABRÉGÉ

L'accélérateur linéaire TrueBeam STx de Varian possède un mode d'utilisation avancé où des plans de traitement peuvent être programmés pour inclure un mouvement de la table où repose le patient pendant le traitement. La combinaison des trajectoires synchronisés de la table de traitement ainsi que du gantry avec la plate-forme d'optimisation RapidArc pour la radiothérapie conformationnelle avec modulation d'intensité volumétrique (VMAT) produit une technique de traitement appelée <<RapidArc avec isocentre virtuel>> (VIRA). En vue de réaliser cette nouvelle technique, la justesse du calcul de dose dans la plate-forme de planification de traitements Eclipse, sur laquelle l'optimisation RapidArc dépend, doit être validée ainsi que la justesse du positionnement de la table de traitement. La justesse du calcul de dose fut évaluée de façon extrinsèque en comparant le résultat de la plate-forme RapidArc pour un plan de traitement de radiothérapie conformationnelle avec modulation d'intensité (IMRT) utilisant un collimateur multilames dynamique (DMLC) à des valeurs mesurés à l'aide d'une chambre d'ionisation ainsi que des films Gafchromic EBT3 en fonction de la distance entre la source et la surface (SSD) d'un phantôme. La dépendence sur SSD de deux paramètres instrinsèques au calcul de dose dans Eclipse, l'écart dosimétrique entre les lames (DLG) et la transmission des lames (LT) fut aussi étudiée. La justesse du positionnement de la table de traitement fut évaluée en produisant des plans de traitements avec la table et le gantry stationnaire, la table stationnaire et le gantry en mouvement ainsi qu'avec le mouvement synchronisé de la table et du gantry, tout en ayant une chambre d'ionisation

positionnée dans un phantôme cylindrique durant la période d'irradiation. L'accord relatif entre les valeurs obtenus de la chambre d'ionisation et ceux d'Eclipse pour les plans DMLC IMRT est descendu de 1.5±0.3% en changeant le SSD de 85 cm jusqu'à 135 cm (moins de 1% de deviation des conditions de références clinique où le SSD est de 100 cm). Les valeurs obtenus à partir des films Gafchromic EBT3 sont en accord avec ceux de la chambre d'ionisation. Par contre, le bruit dans les données du film à basses doses a produit une grande incertitude. En corrigeant pour la projection géométrique, les valeurs du DLG ont été observé comme étant indépendantes du SSD. Le LT a démontré une dépendence sur le SSD de 0.09±0.02% sur la portée de SSD étudiés. Les valeurs de la chambre d'ionisation pour le mouvement synchronisé de la table de traitement et du gantry proposé pour la technique VIRA ont indiqué une déviation maximale de 0.2 cm relativement à l'isocentre du traitement. La même déviation fut observé pour le traitement où la table était stationnaire et le gantry était en mouvement, ce qui correspond aux traitements conventionnels VMAT. Ces résultats démontrent que l'accélérateur linéaire TrueBeam de Varian ainsi q'Eclipse maintiennent la justesse dosimétrique nécéssaire pour les traitements VMAT impliquant des trajectoires dynamiques de la table de traitement.

TABLE OF CONTENTS

LIST OF TABLES

LIST OF FIGURES

Figure page

CONTRIBUTION OF AUTHORS

Results presented in this thesis appear in two manuscripts; one has been submitted to the Journal of Applied Clinical Medical Physics and is under review, and the other is in preparation for submission to Medical Physics. For both manuscripts, I am the primary author, but they have been reviewed and edited by other co-authors. The first is entitled *"Experimental characterization of the dosimetric leaf gap"*, and the pending title for the second is *"Preliminary measurements of Eclipse dose calculation accuracy in the context of dynamic couch trajectories"*. The contribution of authors is as follows:

- Joel Mullins: Assisted in study design, performed experimental work and data analysis, primary author of the manuscripts.
- Alasdair Syme: Principal investigator, provided initial study design and methodology, assisted with interpretation of results and manuscript preparation.
- Jan Seuntjens: provided guidance on study design and interpretation of experimental findings.
- Francois DeBlois: provided guidance on study design and interpretation of experimental findings.

CHAPTER 1
Introduction

1.1 Radiotherapy

Radiation therapy, or radiotherapy, is the application of ionizing radiation to the treatment of disease. The therapeutic benefit of ionizing radiation was realized shortly after the discovery of x-rays at the end of the 19th century [1]. Most frequently it is used in the treatment of malignant disease (cancer) but it can also used to treat certain benign conditions (e.g. trigeminal neuralgia or arteriovenous malformation, among others [2, 3]). Nearly two-thirds of cancer patients will receive some form of radiation therapy during the course of their treatment [4]. The deposition of energy by ionizing radiation into tissue is commonly quantified as absorbed dose, D, defined as the energy absorbed per unit mass. Through years of experiments on cells and animals and clinical trials on humans, clinicians have been able to correlate absorbed dose with both therapeutic benefit and toxicity. Clinical treatment plans are designed based on the experimentally determined therapeutic benefit to maximize the dose to cancerous tissue while respecting dose tolerance thresholds for surrounding healthy tissues and vital organs [5].

Since the advent of radiotherapy, numerous technological advancements have furthered the quality and effectiveness of radiotherapy, including linear accelerators (linacs) to generate higher energy radiation for deeper tissue penetration, and the use

of computed tomography to identify and delineate cancerous tissue to aid in treatment planning [5]. Recently, the standard of radiotherapy care has been evolving rapidly. The development of the multileaf collimator (MLC) played an integral role in the development of intensity modulated radiotherapy (IMRT), in which inverse optimization techniques are used to determine complex MLC-defined field apertures and adjust the beam weight for delivery from multiple incident angles into the patient to better meet planning objectives. Dynamic motion of MLC leaves during radiation delivery increased the achievable degree of intensity modulation in a class of treatments labeled dynamic MLC IMRT, or sliding window IMRT [5]. Volumetric modulated arc therapy (VMAT) treatments incorporate gantry rotation and dose rate variation in addition to dynamic leaf motion to maintain or improve the treatment quality of IMRT while reducing patient treatment time and total radiation output [6]. The decreased treatment time allows for better patient throughput and a smaller risk of intra-fraction positioning errors. Laboratory experiments and radiobiological calculations have suggested that decreasing treatment times may have beneficial radiobiological effects, such as avoidance of tumor cell repair and proliferation [7].

1.2 Varian TrueBeam

The TrueBeam STx linear accelerator (Varian Medical Systems, Palo Alto, CA) introduces further advancements to radiotherapy treatment and research, including a mode that can be used for experimentation in a non-clinical setting while permitting control over all aspects of a treatment delivery. In this research mode, treatments can be programmed that include dynamic couch translation and rotation, gantry

rotation, and collimator rotation during radiation delivery through the specification of control points in an Extensible Markup Language (XML)-formatted file.

1.3 Dynamic Couch Motion

Using this research tool, synchronous couch and gantry motion can be programmed to simulate isocentric treatment with shortened, extended, or variable source-to-axis distance (SAD). In place of the conventional clinical isocenter would be a virtual isocenter that is not fixed in location, but travels in a predefined trajectory while remaining in the beam central axis throughout treatment. With the use of shortened SADs, the distance from the linear accelerator source to the virtual isocenter may be shortened by only 5 cm for complete arcs, but by as much as 30 cm for partial arcs, which would result in a proportional decrease in the projected leaf width of the HD120 MLC at the target volume from its nominal width of 2.5 mm to 1.75 mm. The reduction in effective leaf width offers the potential for more precise, conformal treatment of the target volume. Additionally, the reduced distance from the patient to the x-ray source will yield an increased dose rate, beneficial for stereotactic body radiation therapy (SBRT) and stereotactic radiosurgery (SRS), based on the radiobiological rationale that fewer fractions of higher doses in a shorter overall treatment time results in a more potent biological effect [7, 8, 9]. At extended SAD, the maximum attainable field size is increased which could obviate the need for field junctions. Applications for this approach would include craniospinal irradiation with a Millennium MLC (with maximum 40x40 cm^2 field at SAD = 100 cm) or head and neck cancers with target volumes in the cranial-caudal direction that exceed the MLC-shaped field size limitations of the HD120 MLC (25x25 cm^2 at SAD = 100 cm).

Treatments involving dynamic couch motion have been developed in the past, such as with dynamic stereotactic radiosurgery [10], which used rotations of the treatment couch to treat intracranial lesions using a single noncoplanar arc. More recently, accelerated partial breast irradiation treatments have explored the use of couch rotations to limit dose to the contralateral breast and lung [11, 12]. Another study investigated the addition of dynamic couch and collimator rotation to conventional VMAT treatments using the TrueBeam, generating trajectories in which the overlap between the target volume and critical structures is minimized [13]. Aside from total body irradiation techniques in which longitudinal couch translation is used to uniformly irradiate the entire patient [14], and the use of couch motion to compensate for tumor motion during treatment [15], no notable instances of translational couch motion exist in the literature.

1.4 Varian Eclipse

The Eclipse treatment planning system (Varian Medical Systems, Palo Alto, CA) features a VMAT optimization algorithm called RapidArc. Dose calculations are a necessary component of any VMAT optimization, and in this thesis, the analytical anisotropic algorithm (AAA) is investigated for its dosimetric accuracy under conditions of nonstandard or variable SADs. Measurements obtained during beam commissioning do not typically deviate from standard clinical conditions, and may not be reliable for nonstandard delivery. AAA has been extensively validated for static and modulated deliveries against both measurement and Monte Carlo simulations [16, 17, 18, 19], and for static deliveries at extended source-to-surface distances (SSDs) [20]. In a well-commissioned system, a user can expect that doses calculated

by Eclipse will agree with measurement to within 3% in most circumstances [21]. An investigation of the SSD-dependence of factors related to dynamic MLC treatment deliveries is missing from the literature.

Modulated field dose calculations using AAA require the specification of the leaf transmission (LT) and dosimetric leaf gap (DLG) to accurately model the leakage transmission through the multileaf collimator (LT) and to correct for transmission through the rounded leaf ends featured in Varian MLCs (DLG). Several studies have noted the sensitivity of dose calculation accuracy to errors in the DLG setting. In one investigation, induced systematic errors to the DLG on nine clinical dynamic IMRT plans resulted in between 0.6% and 7.8% dose error per 0.5 mm of induced error [22]. A study reported an increase in the ratio of measured to calculated dose of 1% for every 0.02 cm decrease of the DLG, while another experiment indicated that a 1.0 mm leaf positioning error can result in more than 10% dosimetric error [23, 24]. The presence of a DLG or LT dependence on SSD could significantly affect dose calculations or treatment plan optimization involving dynamic couch trajectories.

The proposed treatment technique combining Varian RapidArc optimization (dependent on Eclipse AAA dose calculations) with dynamic couch trajectories has been designated Virtual Isocenter RapidArc (VIRA). Prior to implementation of this treatment technique in Eclipse, the dosimetric accuracy in the context of dynamic couch motion must be validated. The work presented in this thesis verifies the accuracy of dose calculations using AAA in the Eclipse treatment planning system (TPS) when subject to changes in SSD, by characterizing the extrinsic behaviour

and investigating parameters intrinsic to the dose calculation. Extrinsic evaluation is accomplished through the delivery of clinical DMLC IMRT treatment plans at various SSDs, and measuring the delivered dose using both ionization chambers and radiochromic film. Parameters intrinsic to modulated field dose calculations in Eclipse, the DLG and LT, are characterized for their dependence on SSD.

Additionally, the positional accuracy of the Varian TrueBeam treatment couch is assessed, using ionization chamber current measurements in a cylindrical phantom during continuous radiation delivery involving dynamic trajectories, with comparison to conventional treatment delivery.

CHAPTER 2
Background Information

2.1 Dose Calculation

Critical to the function of a modern radiotherapy clinic is the ability to predict the expected dose distribution accurately from a treatment beam. Forward treatment planning frequently involves repeated dose calculations and adjustments before adequate coverage of the target volume and sparing of healthy tissue is achieved. Inverse planning using computer optimizations also rely on intermediary dose calculations before converging to a solution. In particular, modulated fields frequently consist of small, irregularly shaped fields which can be difficult to model [25].

2.2 Analytical Anisotropic Algorithm (AAA)

The Eclipse treatment planning system (Varian Medical Systems, Palo Alto, CA) employs a pencil beam/superposition model called the anisotropic analytical algorithm (AAA). It is comprised of two components, the configuration algorithm and the dose calculation algorithm.

The configuration algorithm provides the basic physical parameters necessary for the dose calculation, based on the specific accelerator and beam configuration specified in the treatment plan. Initially, a generic data set of physical parameters relevant to dose calculation is selected from a library, pre-computed using Monte Carlo simulations. These are adapted to a specific treatment unit using physical measurements taken during the beam commissioning process, including percentage

depth dose curves, lateral profiles, and output factors for open and wedged fields [17].

When the treatment beam includes modulation using a multileaf collimator, additional values measured during the beam commissioning, the dosimetric leaf gap (DLG) and average MLC leaf transmission (LT), are used in the configuration process. In the generation of a modulated field treatment plan, a leaf motion file is created that describes the position of individual MLC leaves throughout the beam delivery, and this information is used to modify the particle fluence and energy used for the dose calculation based on the specific measurements of the DLG and LT [23].

The output from the configuration algorithm is divided into three radiation components: primary photons generated at the target, secondary photons generated from scattering processes in the linac head, and contaminating electrons. Each component is handled separately in the dose calculation algorithm following division into small, finite-sized beamlets (minimum 1 mm). The computational time is greatly decreased by reducing convolution operations into analytical expressions, made possible due to the use of individual beamlets. The final dose distribution is obtained by superimposing the results from the three radiation components [16].

2.3 Multileaf Collimator Design

Multileaf collimators feature pairs of opposing leaves that are able to translate independently and perpendicular to the beam axis to modulate a radiation field to a specified shape. The dosimetric characteristics of a modulated field are affected by several MLC design considerations. The penumbra width of the radiation field is influenced by the mechanical motion of the MLC leaves. Some vendors opt for

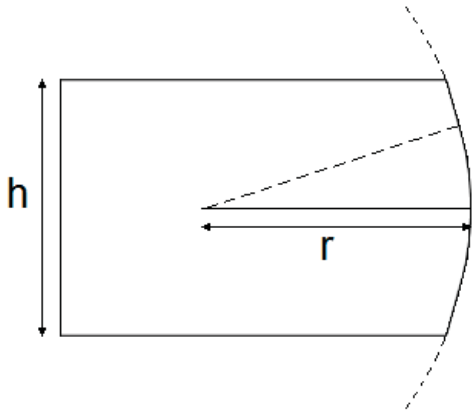

Figure 2–1: Rounded leaf end design of Varian MLC. Millennium MLC features a radius of curvature (r) of 8 cm, and a leaf height (h) of 6 cm. HD120 MLC features a radius of curvature of 16 cm and a leaf height of 6.9 cm.

a focused motion where the leading edge of the leaf matches the beam divergence, whereas Varian MLCs use rectilinear motion for its reduced mechanical complexity [26]. To combat the inconsistent penumbra width as a function of leaf position, rounded leaf edges are used (Fig. 2–1) [23, 27].

2.4 Dosimetric Leaf Gap, Leaf Transmission

As a consequence of the rounded leaf edge design, there is a discrepancy between the geometrically defined field width and the dosimetric field which must be accounted for in dose calculations. This difference is defined as the dosimetric leaf gap (DLG) and can be thought of as an inherent fixed separation of the MLC leaves [24, 28, 29, 30].

Several techniques can be used to estimate the magnitude of the DLG [28]. The integral dose method used in this thesis relates the width of MLC-defined fields

to the integral dose of its profile. Dynamic multileaf collimation is used to create sliding gaps with fixed widths that translate across a jaw-collimated field, with an ionization chamber measuring the integrated charge associated with each profile. Leakage transmission contributes to the measured charge, but can be subtracted for each sliding gap as a function of its width and using an estimate of the average MLC transmission. The corrected charge reading R_{corr} is given by [31]:

$$R_{corr}(g) = R(g) - R_T(g) = R(g) - T_{ave}\left(1 - \frac{g}{l}\right) \tag{2.1}$$

where $R(g)$ is the ionization chamber measurement, and $R_T(g)$ is the leakage transmission component of the charge, estimated using the average MLC transmission T_{ave}, and the gap width g. The total travel distance, l, for all sliding gaps is constant to ensure uniform leaf translation speed for a fixed beam output.

The corrected charge measurements, representing the integral dose for each sliding gap, increases linearly with the gap width. Extrapolating a linear regression fit of the data reveals a nonzero gap width corresponding to zero charge measurement (see Fig. 2–2). This value represents the underestimation of the MLC-defined gap widths with respect to the geometric fields, and is taken as an effective measure of the DLG. The sliding gaps are specified by the treatment delivery plan for their width at isocenter, causing the extrapolated DLG value to be defined under the same conditions.

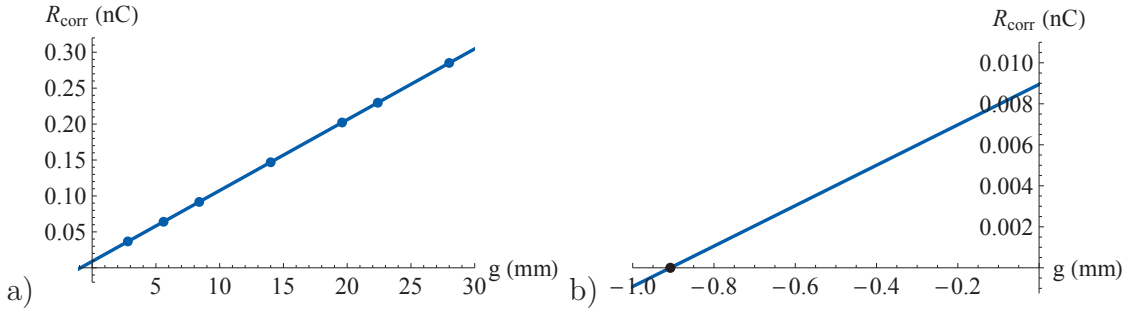

Figure 2–2: a) Linear regression of measured charge R_{corr} as a function of MLC-defined gap width g; b) Extrapolation of the data shows a nonzero gap width corresponding to zero measured charge, defined as the dosimetric leaf gap.

The average MLC transmission T_{ave} is calculated as the average of the charges measured with each MLC leaf banks extended across the entire field while delivering a fixed MU. In addition to the sliding gap and transmission measurements, the charge measured for the open field is also recorded. Leaf transmission (LT) is calculated as a percentage of the open field output:

$$LT = \left(\frac{T_{ave}}{R_{open}} \right) \times 100\% \tag{2.2}$$

2.5 Quality Assurance

Modern radiotherapy involves treatment beams with a high degree of modulation to generate complex dose distributions that conform to the prescribed target volume. To achieve such distributions, IMRT/VMAT treatments employ inverse optimization procedures, which have the potential to generate plans with irregularly shaped or small apertures [25]. The lack of lateral electron equilibrium inherent with these fields

can impact the dose calculation accuracy [29]. Due to the role of dose calculation in each step of iterative treatment plan techniques, dose calculation errors can have a significant impact on the quality of a treatment plan, especially for small target volumes [25, 29]. In addition to dose calculation inaccuracies, systematic geometric errors can lead to significant dosimetric errors [32]. As a result, routine testing of the treatment planning and delivery systems, including patient specific validation, is recommended [21, 33].

As compared to conventional 3DCRT treatment, IMRT involves the delivery of complex dose distributions with steep dose gradients, causing the verification of individual fields to be difficult and inadequate for treatment plan quality assurance (QA). The American Association of Physicists in Medicine (AAPM) Task Group 120 recommends that QA procedures should investigate the delivery of the cumulative treatment plan rather than its constituent fields, by verifying the radiation output with either independent dose calculations software or an absolute dosimeter, and verifying the positions of the gradients relative to one another as well as their absolute position with respect to the treatment delivery coordinates. Several dosimeter options are available: ionization chambers, silicon diodes, and diamond detectors can be used as point dosimeters or arranged into an array and used as spatial dosimeters such as MapCHECK or ArcCHECK (diode; Sun Nuclear, Melbourne, FL), or PTW 2D-ARRAY (ionization chamber; PTW-Freiburg, Germany); radiographic or radiochromic film can also be used as spatial dosimeters [33, 34].

Historically, patient-specific IMRT dose verification was mainly performed using ionization chambers and planar film [34]. In this thesis, ionization chambers and

radiochromic film were used for the measurement of clinical dynamic IMRT treatment plans, and their properties are the focus of the next section.

The complexity of an individual treatment field is related to the degree of beam modulation that is applied. The modulation factor (MF) is a quantity that indicates the influence of the MLC on the delivered dose at a point of measurement, and is defined as the ratio of the dose, D, delivered at the measurement point by the dynamic MLC-collimated field to the open field, while maintaining the jaw-collimated field size and delivered MU [35]:

$$MF = \frac{D_{MLC}}{D_{open}} \tag{2.3}$$

The modulation factor is defined for a single point of measurement, and is therefore dependent on position within the field and may not be indicative of the overall degree of fluence modulation by the MLC.

2.6 Ionization Chamber Dosimetry

Ionization chambers maintain a potential difference between their two electrodes in a gas-filled volume, allowing the collection of charged particles resulting from interactions with the incident ionizing radiation, either created within or entering the ionization chamber volume. Cylindrical ionization chambers feature a central collecting electrode encased in a cylindrical volume. Quantification of the cumulative measured charge is accomplished with the use of an electrometer [36]. The conversion

of measured charge to dose is possible through a calibration coefficient measured or traceable to a national standards laboratory [37].

Due to their finite-sized collecting volume, ionization chambers will exhibit volume averaging effects. When the curvature of the dose distribution is high, as is typically the case with high gradient regions, volume averaging will result in an inaccurate estimation of the dose [33]. Dosimetric accuracy is also dependent on the condition of charged particle equilibrium (CPE), where charged particles exiting the collecting volume are replaced by charged particles entering the volume. The absence of charged particle equilibrium for the irregularly shaped or small apertures present in IMRT fields can perturb the ionization chamber response [38]. For collapsed delivery (fixed gantry angle at 0°) without an opposing beam, a depth dose gradient is unavoidable, but when placed in an otherwise homogeneous region, cylindrical ionization chambers are well suited for IMRT QA as an absolute dosimeter [33]. In this thesis, measurements were taken where the size of the homogeneous dose region was large relative to the ionization chamber, and only minimal deviations to the dose estimates are expected.

Depending on the polarity applied to the ionization chamber, a systematic shift of the collected charge may occur. If operating at a positive polarity, the stimulation of charged particles in the collecting electrode itself will cause a dose-independent increase in the measured charge, whereas the opposite effect will be observed with a negative polarity [36]. The magnitude of this polarity effect is dependent on the properties of the ionization chamber, such as the size of the collecting volume (which affects the magnitude of the measured signal). If the systematic shift is small with

respect to the measured charge, the polarity effect can be ignored. For a 6 MV beam, a polarity correction of more than 0.3% is unlikely [37].

2.7 Radiochromic Film

The active layer in radiochromic film consists of crystalline diacetylenes, which undergo polymerization upon exposure to ionizing radiation [39]. The polymerization induces a monotonic colour change in the film that can be related to the absorbed dose through a sensitometric curve, which describes the film opacity, denoted as optical density (OD), as a function of dose. The optical density is characterized by the relative transmission of light through the film:

$$OD = -\log(T) = -\log\left(\frac{I}{I_0}\right) \tag{2.4}$$

where I is the measured light intensity, and I_0 is the incident light intensity.

Radiochromic film features a monotonically changing colour response to radiation and near water equivalence, marking it as an ideal dosimeter for planar field measurements [40]. Film readout can be performed using commercially available flatbed scanners that measure transmission in each of the RGB colour channels.

Sensitometric curves are characterized by following an established reference dosimetry protocol to deliver absolute doses to film. The nonlinearity between OD and dose with current models of radiochromic film has caused the use of OD to be dispelled in favor of raw pixel values to perform the curve fit [40, 41]. Polynomial

functions have been used traditionally as the model function, but have recently been supplanted by rational functions of the form:

$$PV = a + \frac{b}{D + c} \tag{2.5}$$

where PV is the measured pixel value, D is the dose, and a, b, c are fit parameters. Functions of this form better match the film behaviour due to the forced monotonicity [40].

2.7.1 Multichannel Dosimetry

Single channel dosimetry is based on the dose-response behaviour of individual colour channels, where the sensitivity is indicated by the magnitude of the calibration curve slope. A steep gradient exhibits good dose resolution while mitigating the influence of pixel value measurement errors. It has been suggested to select a colour channel based on its respective sensitivity in the dose region being examined [42].

However, single channel dosimetry methods may suffer from film inconsistencies and scanner artifacts. Multichannel dosimetry methods have emerged that are able to separate the signal into dosedependent and independent components, allowing for corrections to these effects. Following the initial suggestions by Micke *et al.*, a multichannel dosimetry method was delineated by Mayer *et al.* that used each colour channel and their calibration curve gradients to minimize a cost function, arriving at a single estimation of the dose [43, 44]. Their cost function was:

$$\Omega(i,j) = \sum_{k\neq m}^{3} ((D_k(i,j) + a_k(i,j)\Delta(i,j)) - (D_m(i,j) + a_m(i,j)\Delta(i,j)))^2 \qquad (2.6)$$

where D_x refers to the dose estimates for each of the RGB colour channels, a_x is the slope of their calibration functions at that point, and Δ is the minimization parameter. Minimizing this function ($\frac{\mathrm{d}\Omega}{\mathrm{d}\Delta}(i,j) = 0$) yields the solution:

$$\Delta(i,j) = -\frac{\sum_{k\neq m}^{3} (D_k(i,j) - D_m(i,j))(a_k(i,j) - a_m(i,j))}{\sum_{k\neq m}^{3} (a_k(i,j) - a_m(i,j))^2} \qquad (2.7)$$

leading to a dose estimate optimized for the relative gradients from each channel:

$$D(i,j) = \frac{1}{3}\sum_{k\neq m}^{3} (D_k(i,j) + a_k(i,j)\Delta(i,j)) \qquad (2.8)$$

The use of film as an absolute dosimeter can be problematic due to variations in the dose response between different production lots and even within the same batch. There is no generic calibration function that can be used for all radiochromic films. Lewis *et al.* presented a method to adapt the response of films to a calibration curve, within the same lot using a simple two-point rescaling, but did not advise the use of this method between different lots [40].

CHAPTER 3
Materials and Methods

3.1 Dosimetric Leaf Gap, Transmission

DLG was measured following Varian recommendations [31]. The multileaf collimator was used to define gaps with widths ranging from 2 mm to 20 mm, which were translated across a 10×10 cm^2 field (Fig. 3–1). For each gap width, 100 monitor units were delivered, with each leaf traveling a total of 120 mm at a uniform speed. Charge was measured by an ionization chamber at depth in a water-equivalent phantom, positioned with the orientation of the chamber perpendicular to the direction of MLC leaf travel. An estimate of leaf transmission was obtained by averaging measurements with each leaf bank extended across the entire field, with the ionization chamber positioned as with the sliding gap measurements. The experimental setup is illustrated in Fig. 3–2.

DLG was measured at SSDs between 80 cm and 140 cm in 5 cm increments, for a Varian ClinaciX linac equipped with a Millenium MLC and a Varian Trilogy linac equipped with a HD120 MLC, at both 6 MV and 18 MV energies (Varian Medical Systems, Palo Alto, CA). MLC specifications are listed in Table 3–1. The two machines are beam-matched for both energies (6 MV: iX PDD10 = 66.4%, Trilogy PDD10 = 66.6%; 18 MV: iX PDD10 = 79.3%, Trilogy PDD10 = 79.2%). Profiles at depth of maximum dose for both energies on both machines agree to within 0.5% across the inner 80% of the maximum field size (40×40 cm^2). Measurements

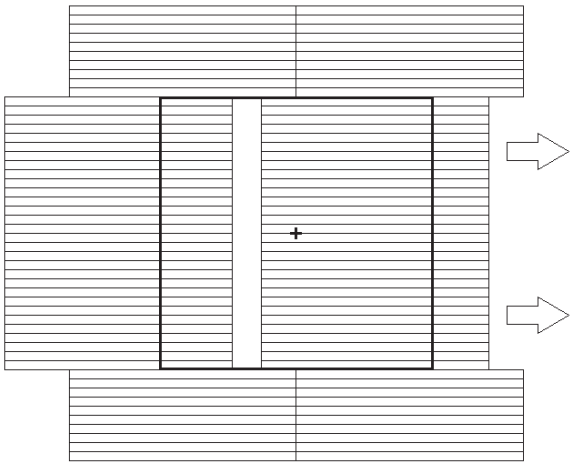

Figure 3–1: Integral dose (sliding gap) DLG measurement. Gaps defined by MLC leaves of increasing width are translated across a 10×10 cm^2 field as a fixed number of MUs is delivered. Charge is measured with an ionization chamber in water-equivalent phantom, oriented perpendicular to the direction of leaf travel.

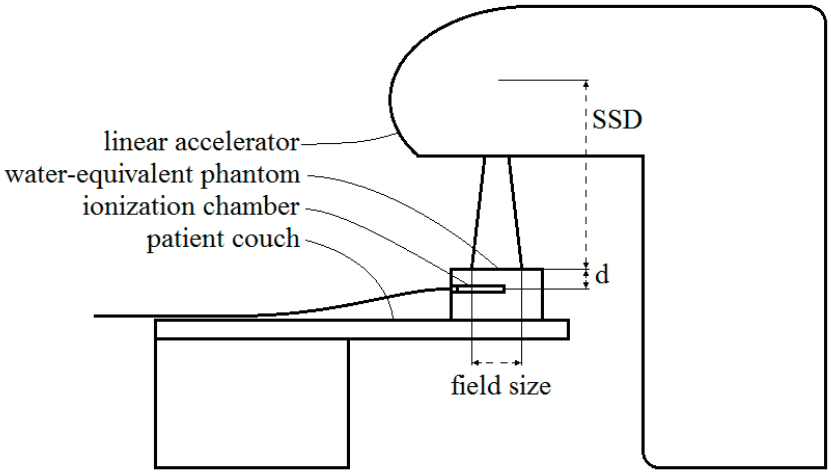

Figure 3–2: Diagram of the experimental setup. DLG was measured with an ionization chamber at depth d in a water-equivalent phantom for a range of SSDs. Pictured is a cross-section with the ionization chamber located inside the phantom.

Table 3–1: Multileaf collimator specifications for leaf thickness, radius of curvature of rounded leaf ends, and leaf width at isocenter.

Multileaf Collimator Specifications			
Model	Leaf Height (cm)	Leaf end radius (cm)	Leaf width (mm)
HD120 MLC	6.9	16	2.5/5 (inner/outer)
Millennium MLC	6.0	8	5

Table 3–2: Specifications of collecting volume and chamber radius for ionization chambers used for DLG measurements.

Ionization Chamber Specifications		
Chamber	Cavity Radius (cm)	Collecting Volume (cm^3)
NE2571	0.315	0.60
ExradinA12	0.305	0.65
NE2577	0.315	0.20
PTW31010	0.275	0.125

were taken using four different ionization chambers (see Table 3–2), at 5 cm and 10 cm depths in a water-equivalent phantom. NE2571 (QADOS, Sandhurst, UK) and ExradinA12 (Standard Imaging, Middleton, WI) ionization chambers were used for measurements on each linac. The ionization chambers used for routine clinical IMRT QA were used only on their designated linacs, with an NE2577 (QADOS, Sandhurst, UK) chamber used on the ClinaciX, and a PTW31010 (PTW-Freiburg, Freiburg, Germany) used on the Trilogy. For SSDs between 80 cm and 110 cm, a calibrated pointer was used to set the couch position. For SSDs greater than 110 cm, the COUCHVRT value displayed by the console was used as a reference. DLG was also measured on the HD120 MLC for dose rates ranging from 100-600 MU/min, obtained at an SSD of 110 cm and a measurement depth of 10 cm, using the NE2571 ionization chamber.

To maintain consistent experimental conditions, the measurements were divided into categories, separated by linac type, measurement depth, and energy. During each measurement period, only the ionization chamber being used and the SSD were altered.

Corresponding dose calculations were simulated in Eclipse for beam energy 6 MV and measurement depth 5 cm for both the ClinaciX and Trilogy linear accelerators.

3.2 Polarity Effect

Polarity effects were quantified for their impact on DLG measurements on the Trilogy linear accelerator. The water-equivalent phantom was positioned at an SSD of 135 cm to maximize the detectable effect due to the lessened magnitude of the measured charge at these distances. To assess the polarity effect, measurements were taken at opposing voltages of +300 V and -300 V for the PTW31010, NE2571, and ExradinA12 ionization chambers.

3.3 Dynamic IMRT Verification

3.3.1 Ionization Chamber Measurements

Verification plans with collapsed gantry, collimator and couch rotation angles were generated from eleven clinical DMLC IMRT plans with treatment on either a Varian ClinaciX equipped with a HD120 MLC, or a Varian Trilogy equipped with a Millennium MLC.

The verification plans were delivered to a water-equivalent phantom at SSDs ranging from 85 cm to 135 cm in increments of 5 cm. A calibrated pointer was used to set the couch position for SSDs up to 110 cm. For SSDs greater than 110 cm, the COUCHVRT value displayed by the console was used as a reference.

Ionization chamber measurements were recorded for a depth of 5 cm in the beam central axis using an NE2577 chamber on the ClinaciX and a PTW31010 chamber on the Trilogy, similar to the DLG and LT measurements in Fig. 3–2. In the Eclipse TPS, corresponding dose calculations were performed for each patient, and the dose estimates for a verification point at 5 cm depth were recorded. Eclipse TPS screenshots of the dose calculations in Eclipse on the water-equivalent phantom are illustrated Fig. 3–3 for a verification plan corresponding to the clinical treatment plan illustrated in Fig. 3–4.

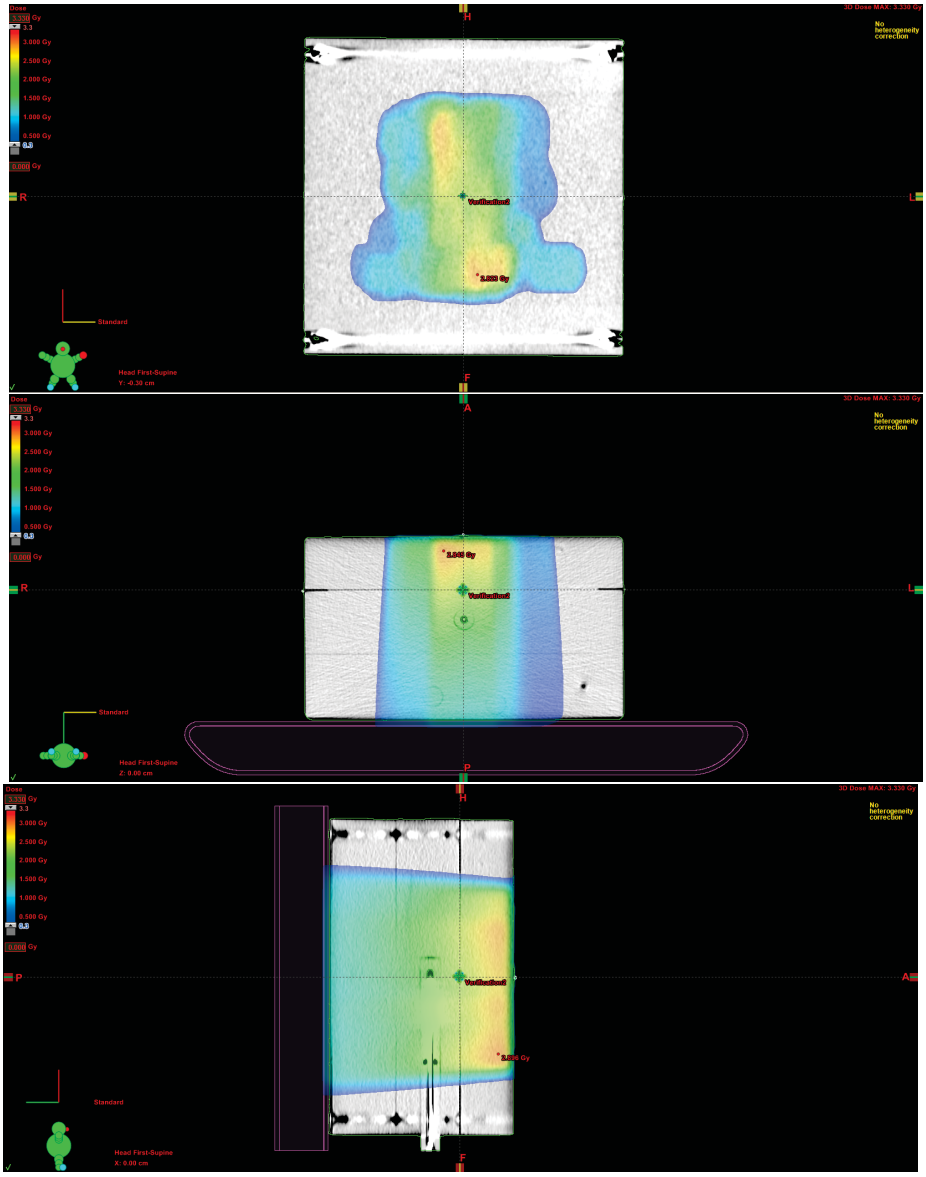

Figure 3–3: Eclipse TPS screenshots of coronal (top), transverse (middle) and sagittal (bottom) planar cross-sections for the simulation of a left abdominal wall dynamic MLC IMRT verification plan delivered to a water equivalent phantom. The plan was recalculated a function of SSD, and the dose estimate at the reference point labeled Verification2.

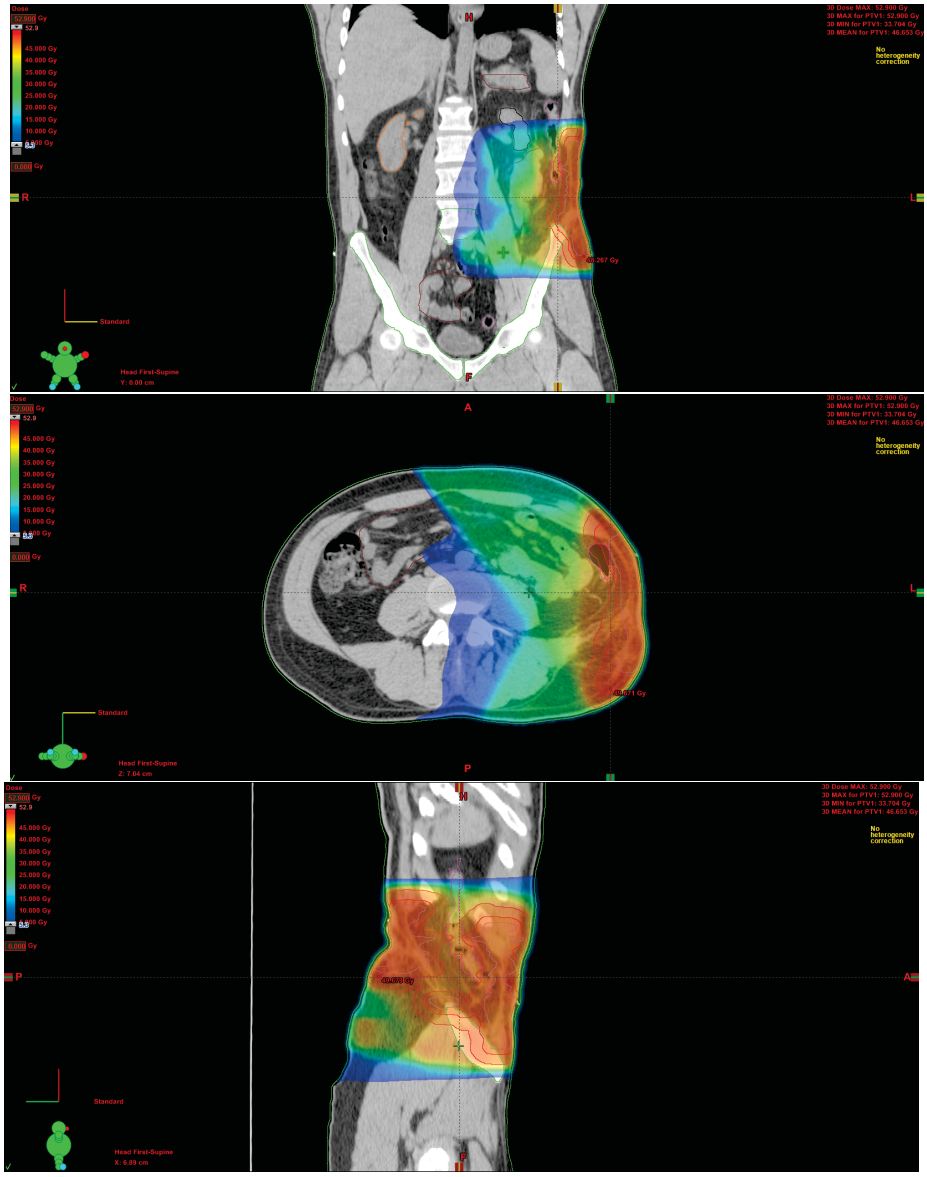

Figure 3–4: Eclipse TPS screenshots of coronal (top), transverse (middle) and sagittal (bottom) planar cross-sections for dose calculations of a left abdominal wall treatment using dynamic MLC IMRT.

3.3.2 Radiochromic Film Measurements

Treatment verification plans were also delivered to Gafchromic EBT3 film (Ashland Specialty Ingredients, Covington, KY) at 2 cm depth in water-equivalent phantom at both 85 cm and 135 cm SSD. An Epson 10000XL scanner was used to scan the films in transmission mode as 48-bit .tif images with 150 dpi resolution. Calibration data consisted of 16 films irradiated with known doses between 0 Gy and 25 Gy within the same lot as the measurement films, and scanned under the same conditions. A film-sheet specific calibration was performed with an additional calibration dose delivered under clinical reference conditions (SSD = 100 cm, field size = 10x10 cm^2, with film placed at depth of maximum dose = 1.5 cm) to a strip cut from the same film sheet on which the verification plan was irradiated [40]. MATLAB code for the multichannel dosimetry described in Eq. 2.6 - 2.8 was developed for pixel value to dose conversion [43, 44]. Planar dose profiles corresponding to the film measurement conditions were exported from Eclipse TPS for the purpose of comparing planned and delivered dose distributions.

3.4 Positional Accuracy

As a preliminary test of radiation delivery under conditions of dynamic couch motion, treatment beams were programmed using the TrueBeam developer's mode. Couch and gantry positions were specified as a function of delivered MU using the XML schema for the developer's mode. Three plans were generated: stationary couch and gantry, stationary couch and rotating gantry, and circular couch rotation with a 5 cm radius in synchrony with gantry rotation. 1800 MU were delivered in total for each plan, with a 10×10 cm^2 field, and at a dose rate of 600 MU/min. An

ionization chamber was placed in the center of a cylindrical phantom and positioned at the virtual isocenter, and the current was recorded each second during radiation delivery on the TrueBeam.

CHAPTER 4
Results

The results in this chapter outline the observed dependencies for dosimetric leaf gap (DLG) and leaf transmission (LT) measurements on SSD, MLC model, ionization chamber, depth of measurement, energy, and dose rate. A manuscript presenting the characterization of the DLG for these dependencies has been submitted to the Journal of Applied Clinical Medical Physics.[1]

Measurements obtained from the delivery of dynamic MLC IMRT verification plans to ionization chamber and radiochromic film are presented, as well as open field dose measurements, for their dependence on SSD. A correlation between individual field dependencies and modulation factor was also investigated. An article detailing the dependence of IMRT verification results, DLG, and LT on SSD in the context of dynamic couch trajectories is in preparation for submission to Medical Physics.

4.1 Dosimetric Leaf Gap, Leaf Transmission

4.1.1 Dosimetric Leaf Gap

In this work, each DLG measurement was obtained from the linear regression of seven sliding gap charge measurements as a function of the gap width, and subsequent extrapolation to the abscissa to identify the gap corresponding to zero measured

[1] J. Mullins, J. Seuntjens, F. DeBlois, A. Syme, "Experimental characterization of the dosimetric leaf gap," *Journal of Applied Clinical Medical Physics*, submitted

charge. For each estimate of the DLG, linear regression yielded an R^2 coefficient greater than 0.9999, indicating consistent proportionality of the charge measurements to the gap width within a single estimation of the DLG. To assess reproducibility, ten repeated measurements were performed in series, each immediately following the last, without any changes to the experimental conditions, The standard deviation of these measurements was 1.03%, suggesting that any noise in the measurements results from variations in the setup conditions rather than the measurement itself. Error bars would be indiscernible on the following figures showing the DLG results, and are omitted.

Seven ionization chamber measurements were used in the linear regression for each DLG estimate. The high correlation indicated by the R^2 coefficients suggests that seven data points may be excessive to accurately characterize the DLG. To assess this, each DLG measurement was recalculated using only the charge measurements for the 2 mm and 20 mm gaps, and compared to the DLG defined by seven charge measurements. On average, the DLG defined by two data points differed by 1.3±0.8%, corresponding to a length of less than 0.02 mm at isocenter.

For all figures showing DLG results, faded points correspond to raw DLG measurements. Unfaded points correct for the geometric projection of the DLG for its magnitude at isocenter (100 cm). To be better able to discern the effect of measurement depth, the data are plotted for the distance from the x-ray source to the point of measurement rather than SSD.

Fig. 4–1 compares the DLG measurements for each ionization chamber used for the Millennium and HD120 MLC. These measurements are also illustrated in

Fig. 4–2, but rearranged to illustrate their dependence on depth of measurement in phantom. The DLG estimates obtained with the PTW31010 ionization chamber were greater than the large volume chamber measurements by 0.04 mm on average. Measurements on the HD120 MLC at 18 MV differed at the investigated depths, but each ionization chamber yielded DLG estimates that agreed within 0.08 mm for the two depths. Similarly, the DLG measurements obtained using the NE2577 ionization chamber on the Millennium MLC were greater at a depth of 10 cm compared to 5 cm, but agreed within 0.08 mm.

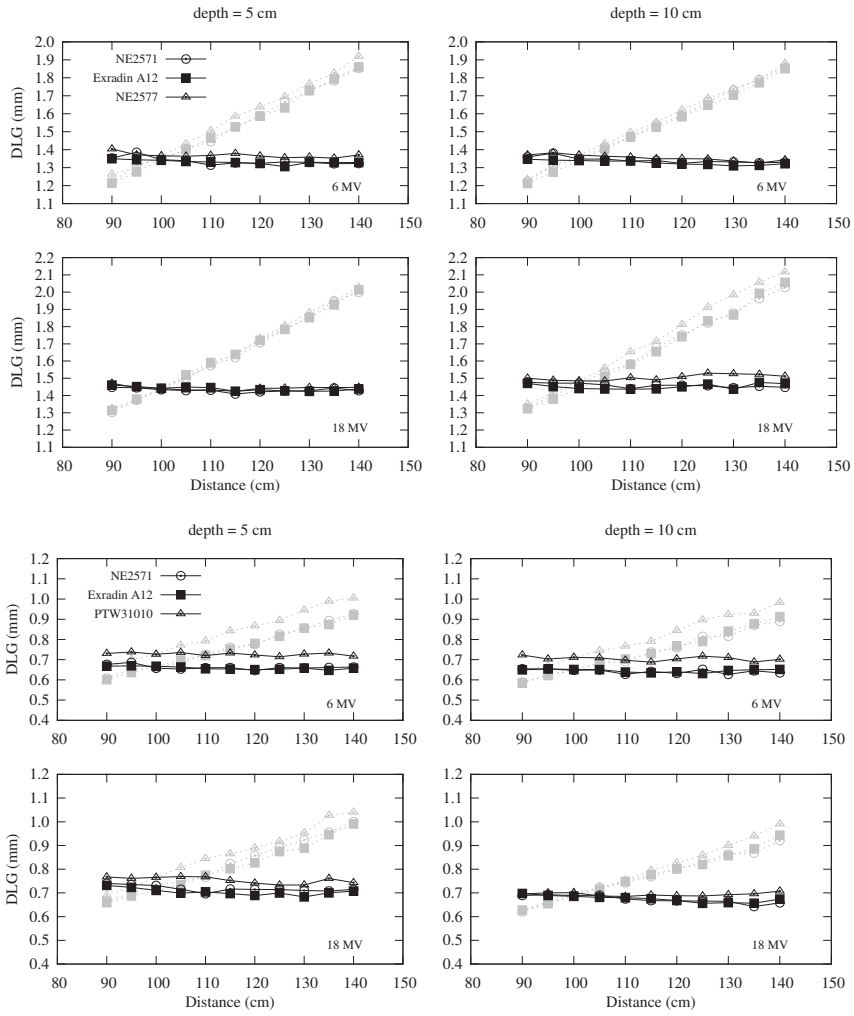

Figure 4–1: Millenium MLC (top) and HD120 MLC (bottom) DLG measurements for three ionization chamber types: NE2571, ExradinA12 and NE2577. Left: measurements taken at 5 cm depth; Right: measurements at 10 cm depth; Top: beam energy 6 MV; Bottom: beam energy 18 MV. As a measurement of length, the DLG is subject to geometric projection as the distance from the linac source increases. Unfaded data points show corrected values. Data is plotted for the distance from the x-ray source to the point of measurement.

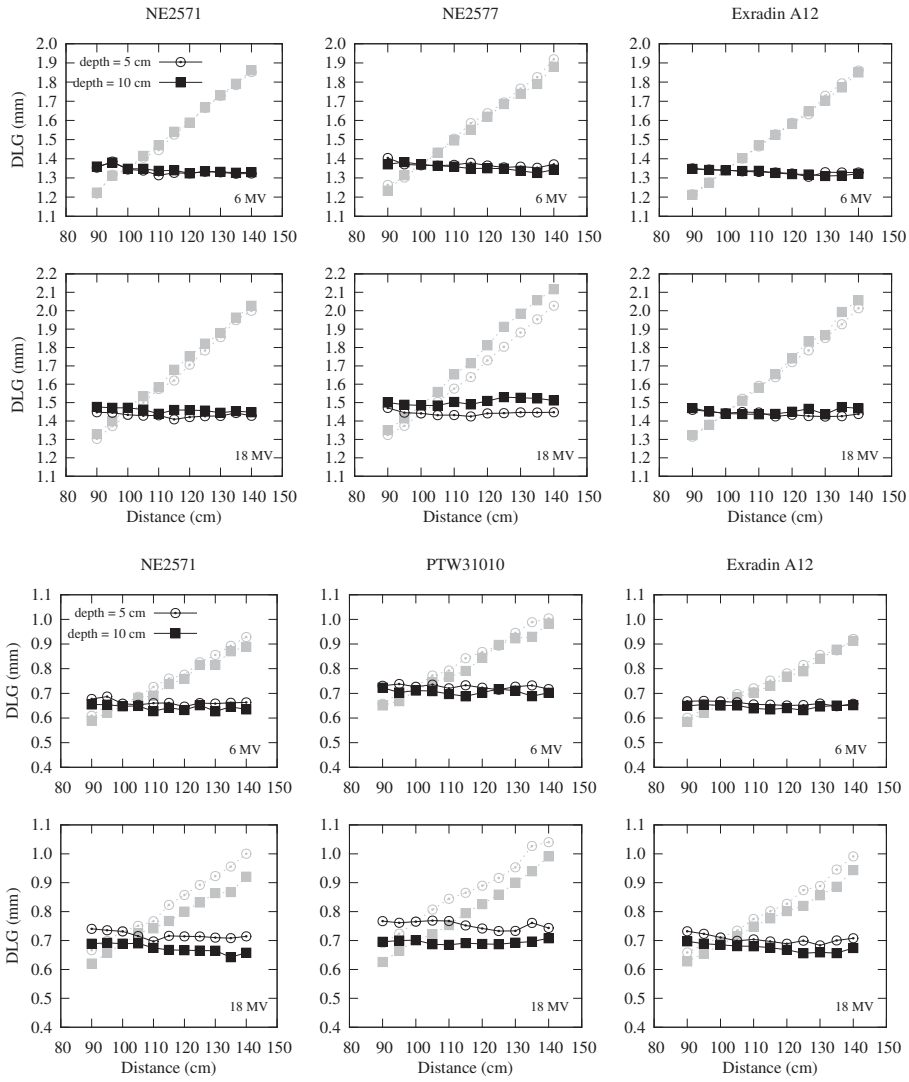

Figure 4–2: Millennium MLC (top) and HD120 MLC (bottom) DLG measurements, dependence on measurement depth. Labels indicate ionization chamber used for measurement. Unfaded points show measured DLG values following correction for geometric projection. Data is plotted for the distance from the x-ray source to the point of measurement.

For each set of DLG measurements, linear regression was used to assess the dependence on SSD. The slope of each regression line was tested for a statistically significant difference from zero, using a t-test. For the 24 datasets (3 ionization chambers per linac, 2 energies, 2 depths, 2 MLC models), 15 were found to have a statistically significant dependence on SSD ($p < 0.05$). The p-values obtained through the regression analysis are plotted as function of the slope in Fig. 4–3, and categorized by ionization chamber, energy, depth and MLC model. No evident pattern is observed to link the DLG dependence on SSD to these parameters. The results of the linear regression indicate that for every metre change in SSD, the measured DLG value will vary by less than 0.1 mm.

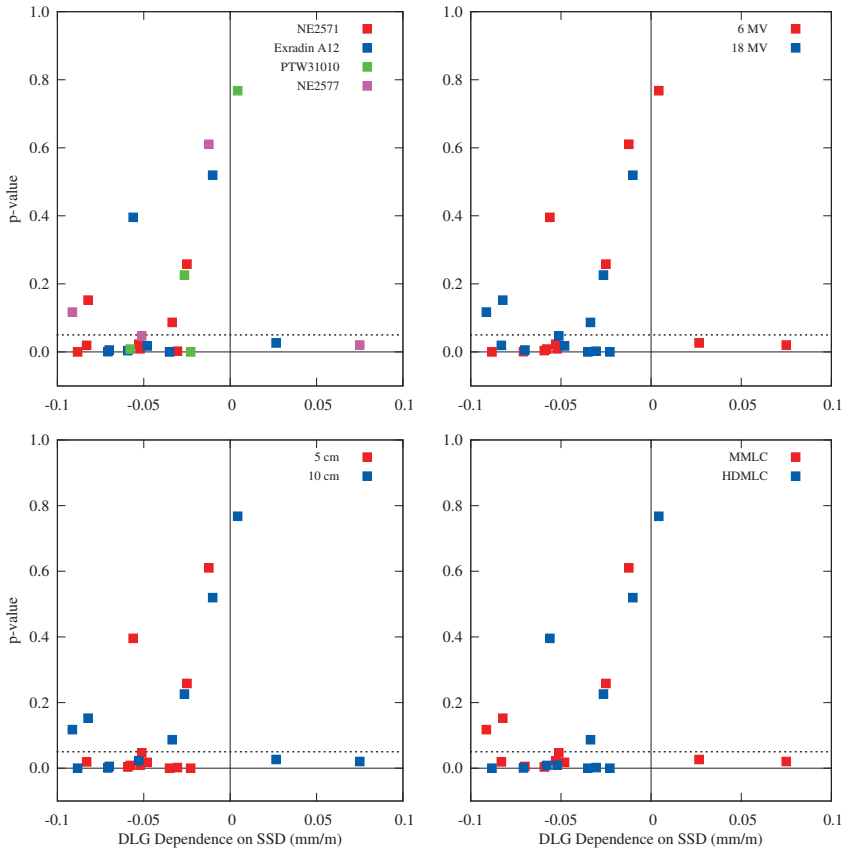

Figure 4–3: Statistical significance of the DLG dependence on SSD (in millimetres of DLG per metre of SSD) was evaluated using a t-test for each DLG dataset. Using a criteria of $p<0.05$, 15 of the 24 datasets showed a statistically significant dependence of DLG on SSD. These graphs show the p-values obtained through this analysis plotted as a function, and coloured based on ionization chamber (top left), energy (top right), depth of measurement (bottom left), and MLC model (bottom right). No evident pattern is observed to link the slope to any of these categories. Dashed line indicates the t-test criteria; points below this line show a statistically significant dependence on SSD.

Due to the absence of a clinically relevant dependence on SSD, apart from geometric projection, the standard deviation of the geometrically corrected DLG measurements was calculated for each combination of multileaf collimator, energy, ionization chamber, and depth. The average standard deviation, given as a percentage due to the varying magnitude of the DLG under each set of experimental conditions, was (1.31±0.09)%.

4.1.2 Leaf Transmission

Leaf transmission (LT) measurements are shown in Fig. 4–4 for their dependence on ionization chamber model, and again in Fig. 4–5 for their dependence on the depth of measurement. Across the SSD range investigated, the LT measurements vary on average by (-0.09±0.02)%. When comparing LT for the same point of measurement but at different measurement depth, the difference was more pronounced at 6 MV than at 18 MV (see Fig. 4–5), with an average difference of (0.04±0.01)% at 6 MV compared to (-0.002±0.007)% at 18 MV.

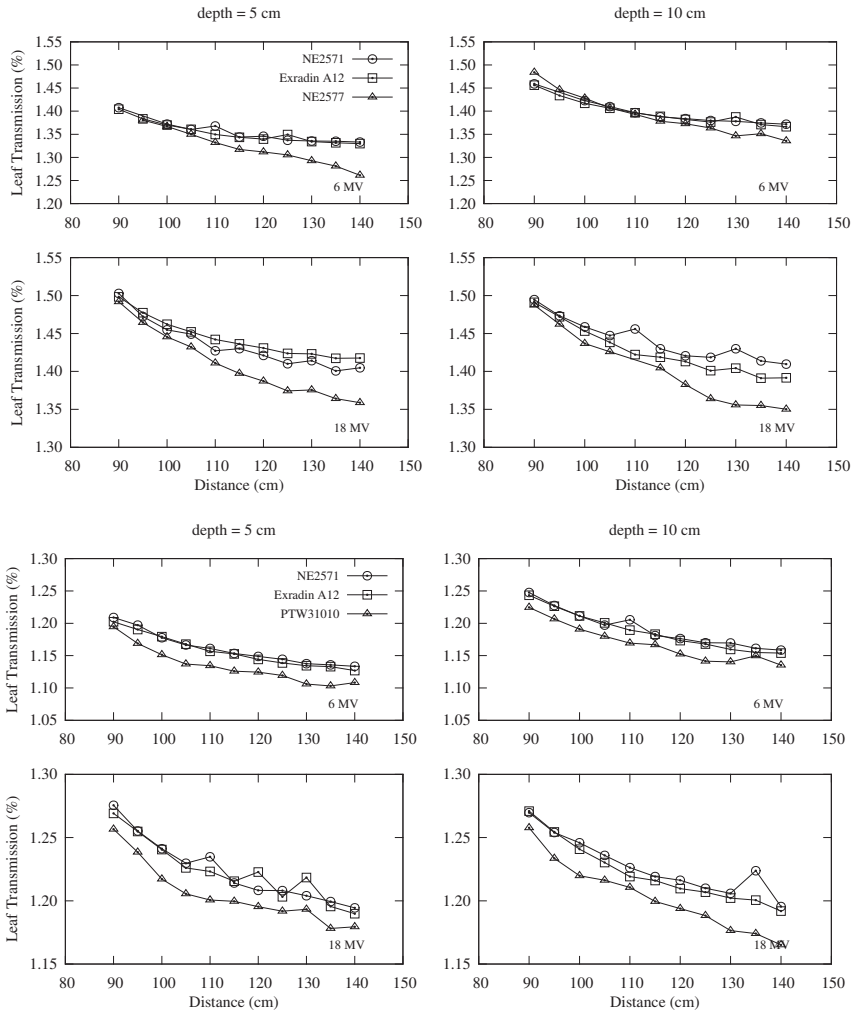

Figure 4–4: Millennium MLC (top) and HD120 MLC (bottom) LT measurements for three ionization chamber types: NE2571, ExradinA12 and PTW31010. Left graphs show measurements taken at a depth of 5 cm in water-equivalent phantom, right graphs showing measurements at a depth of 10 cm. Upper graphs are taken at 6 MV, lower graphs are taken at 18 MV. Data is plotted for the distance from the x-ray source to the point of measurement.

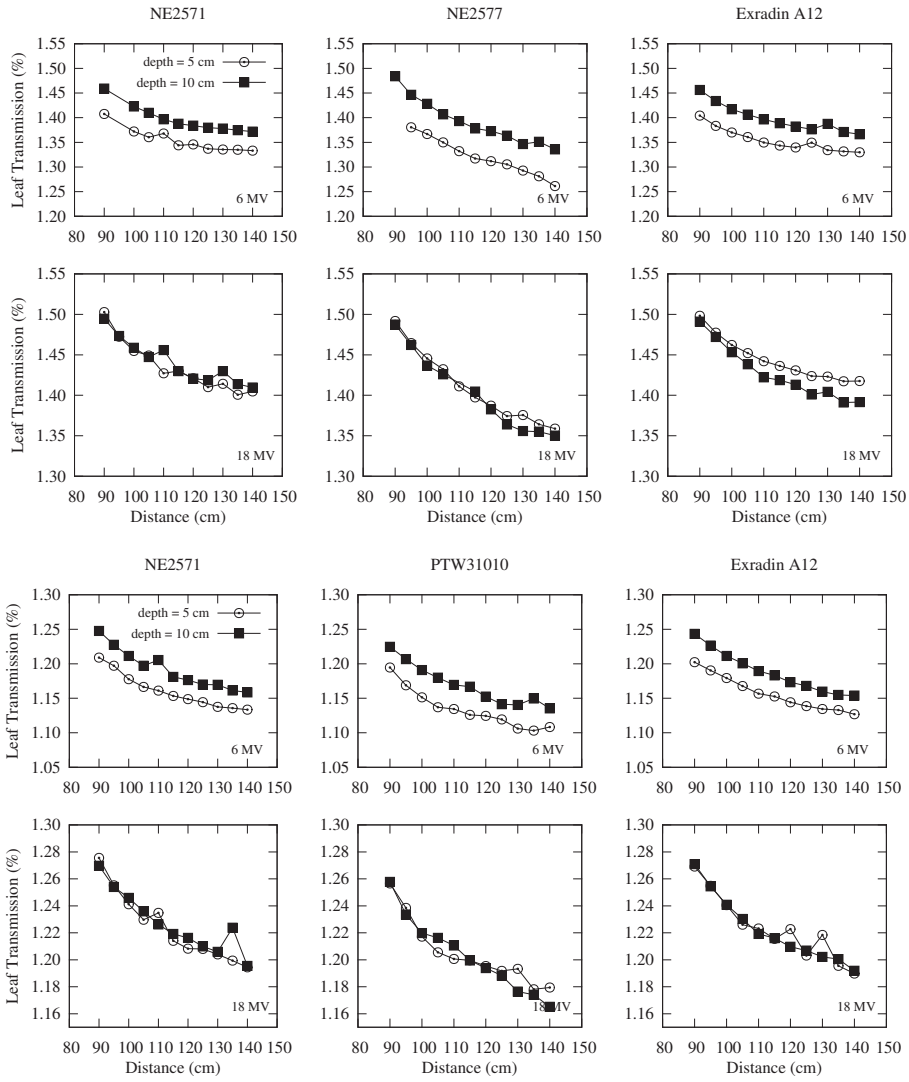

Figure 4–5: Millennium MLC (top) and HD120 MLC (bottom) LT measurements, dependence on measurement depth. Labels at the top indicate ionization chamber used for measurement. Data is plotted for the distance from the x-ray source to the point of measurement.

The DLG measurements taken as a function of dose rate are illustrated in Fig. 4–6. Linear regression of the data was analyzed with a t-test, and yielded no statistically significant dependence of DLG on dose rate (p ¿ 0.05).

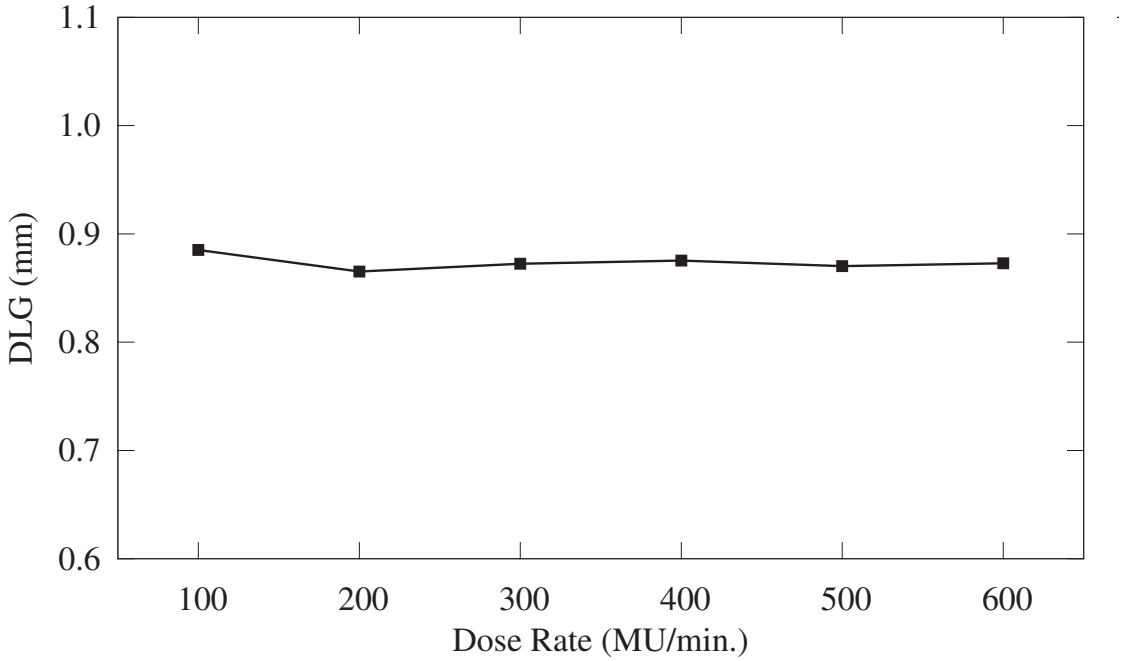

Figure 4–6: DLG dependence on dose rate. Measurements were taken at an SSD of 110 cm, using an NE2571 ionization chamber placed at 10 cm depth in water-equivalent phantom, at beam energy 18 MV, and with HD120 MLC.

4.2 Dynamic IMRT Verification

4.2.1 Ionization Chamber Measurements

The relative agreement between ionization chamber measurements and Eclipse dose calculations as a function of SSD for the cumulative treatment plan dose is shown

in Fig. 4–7, renormalized at 85 cm SSD for better visualization of the dependence on SSD. The bold line depicts the average relative agreement for each SSD. Comparing the relative agreement at 85 cm SSD and 135 cm SSD, there is an average decrease of (1.5±0.3)%. As this data is normalized for agreement at 85 cm SSD, this corresponds to less than a 1% deviation for all SSDs compared to standard clinical conditions (100 cm SSD).

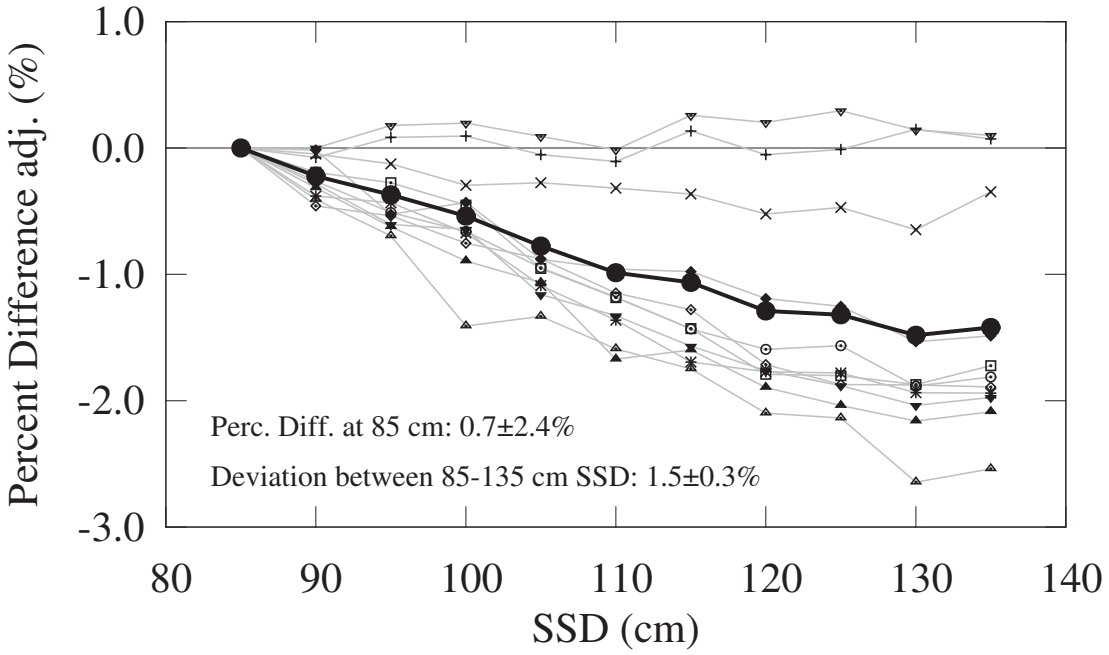

Figure 4–7: Dynamic MLC IMRT verification plan delivery measurements with ionization chamber. For measurements of clinical treatment plans, agreement was renormalized at 85 cm SSD, with an average agreement before renormalization of 0.7±2.4%. The large black points indicate the average of the normalized measurements at each SSD. Applying a linear fit to the averaged data resulted in a deviation of 1.5±0.3% in the 85-135 cm SSD range.

In addition to the cumulative dose from each collapsed delivery treatment plan, the dose was both measured and calculated in Eclipse for each individual field. The relative agreement between the ionization chamber measurements and the Eclipse dose calculations was calculated, and the dependence on SSD was estimated through

the slope of a linear fit. This slope data was plotted as a function of the modulation factor for each field in Fig. 4–8.

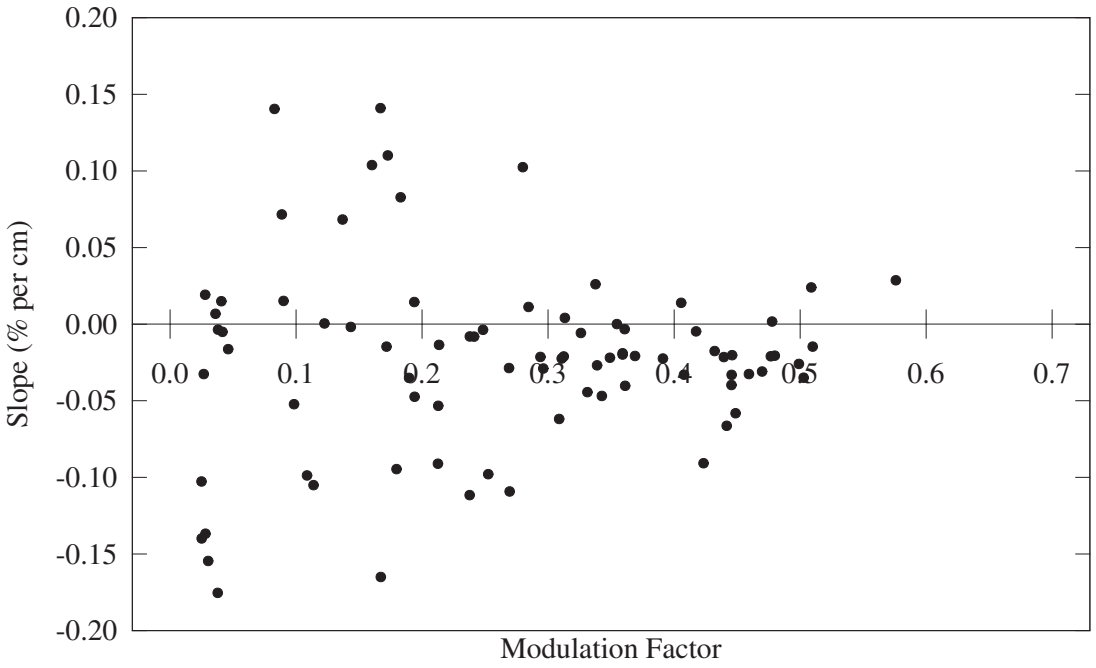

Figure 4–8: Dependence of the percentage agreement of calculated dose compared to measured dose as a function of SSD for individual dynamic MLC IMRT fields plotted against the field modulation factor.

For each sub-field, the relative agreement was weighted by the measured dose for the individual field relative to the cumulative plan dose at each SSD. From the weighted percentage agreement, linear regression was again used to obtain the dependency on SSD as represented by the slope. A minimum dose threshold of 10% of the cumulative plan dose at a given SSD was enforced for each field, such that data

points not fulfilling this condition were excluded. The resulting dataset is illustrated in Fig. 4–9.

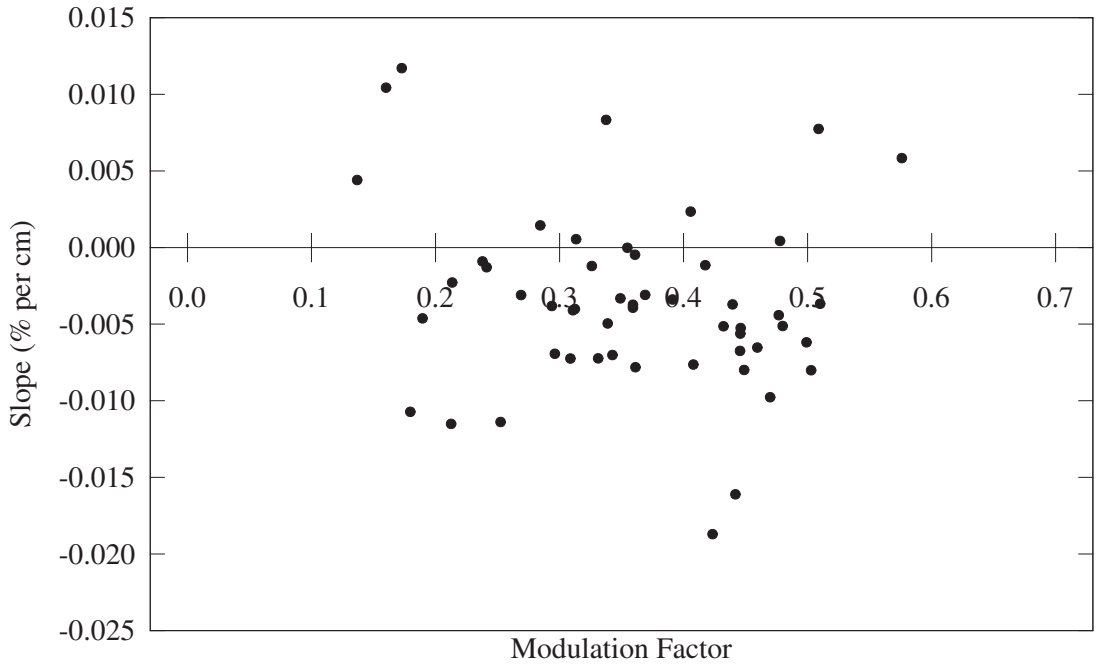

Figure 4–9: Weighted relative agreement dependence on SSD for individual fields as a function of field modulation factor. Data points shown in Fig. 4–8 were selectively removed based on a minimum dose threshold for the individual field dose relative to the cumulative plan dose at each SSD.

4.2.2 Radiochromic Film Measurements

Following registration of the dose distributions measured with film and calculated in Eclipse, the percentage difference was calculated for each pixel. To compare the relative agreement at 85 cm and 135 cm SSD, regions corresponding to the same

projected area of the radiation beam were used. This was accomplished by separating the pixels for the 135 cm SSD data into dose bins, creating logical masks corresponding to the pixels that lie within each bin, and backprojecting these delineated regions to the 85 cm SSD plane. The average relative agreement within these regions at 85 cm and 135 cm SSD as a function of dose is shown for each plan in Fig. 4–10, with the error bars denoting the standard deviation. The dose levels indicated refer to the dose distribution at 135 cm SSD.

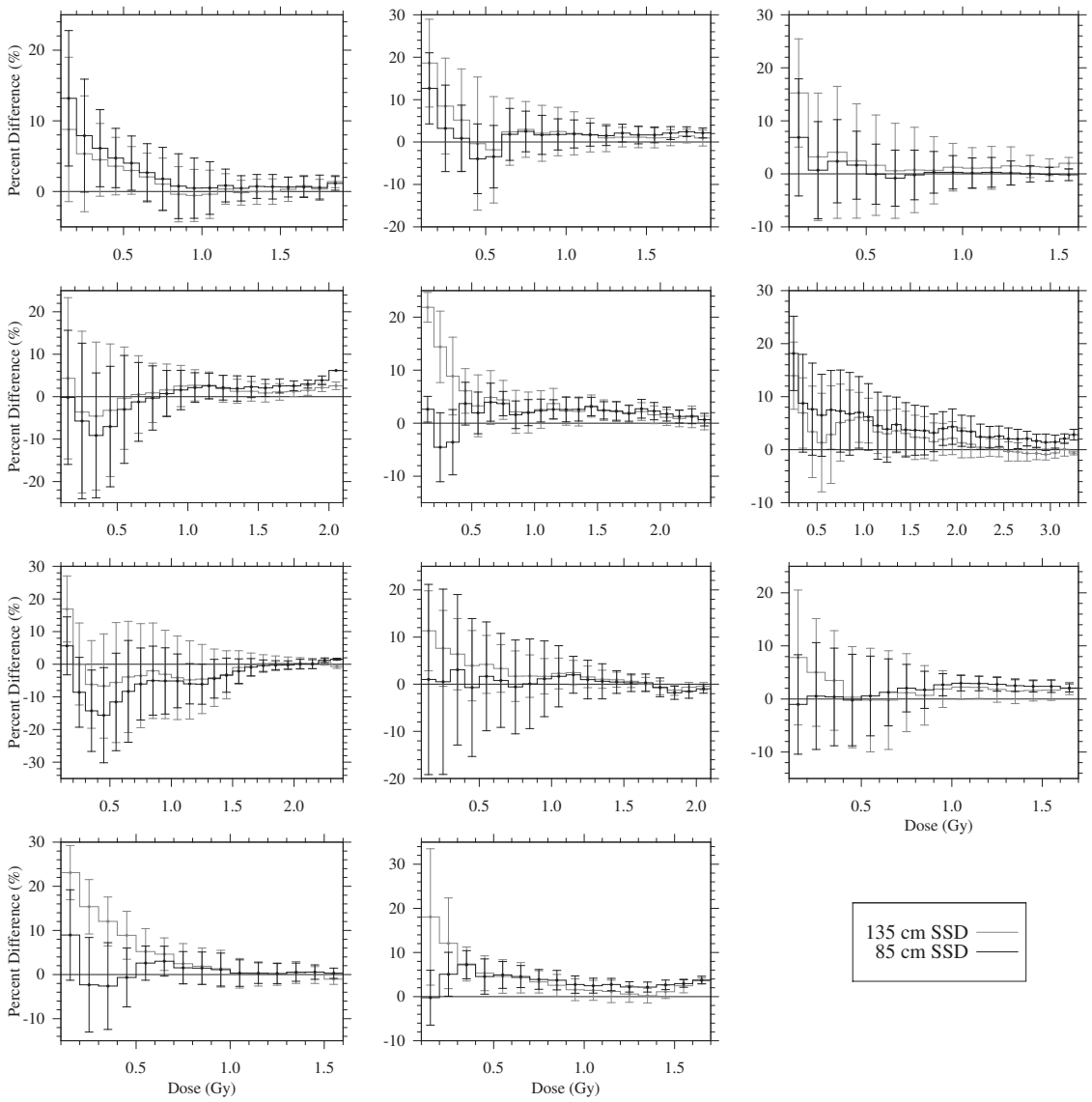

Figure 4–10: For each treatment plan irradiated to film at 85 cm and 135 cm, the agreement within the same projected area was averaged, and separated by dose levels (defined at 135 cm SSD). Error bars denote the standard deviation of the measured data within each dose bin.

For each dose bin, the difference between the relative agreement at 135 cm SSD and 85 cm SSD was calculated, and averaged for all patients. Fig. 4–11 shows the average agreement for all patients within each dose bin defined at 135 cm SSD.

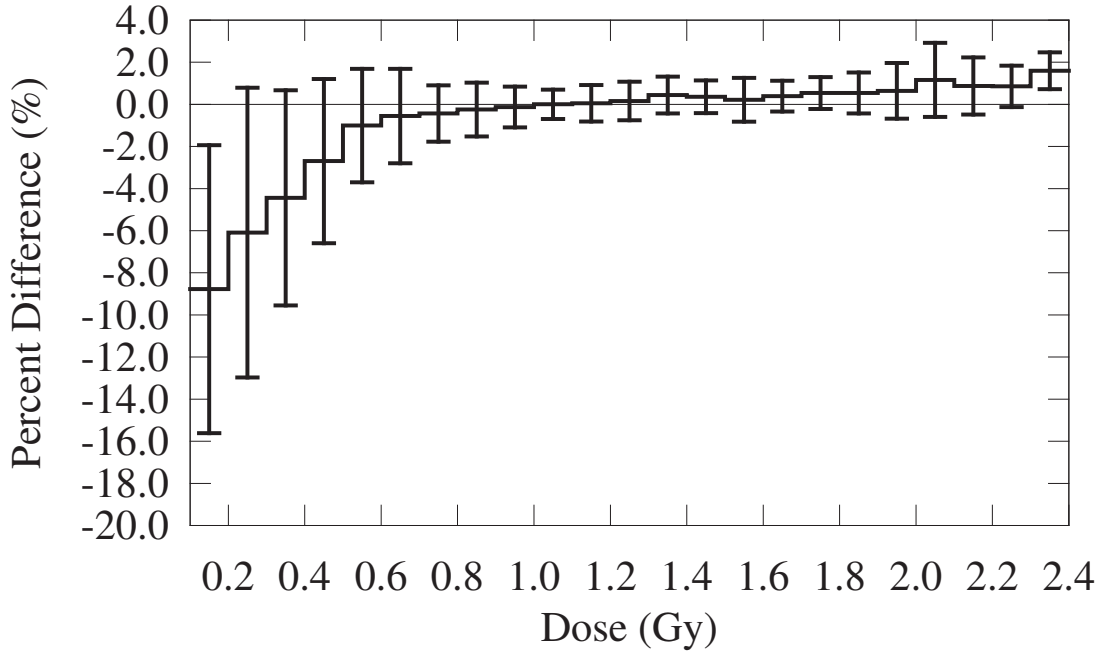

Figure 4–11: The difference in the agreement between films irradiated at 135 cm and 85 cm SSD for each treatment plan and dose bin was calculated. The average difference in agreement for each dose bin is shown here, where a positive value corresponds to a higher measured dose at 135 cm SSD. Error bars denote the standard deviation of the averaged data.

4.3 Positional Accuracy

The current measurements obtained to assess the positional accuracy of the couch was normalized to the maximum value for each trajectory, and plotted as a function of gantry rotation angle in Fig. 4–12. For the rotating gantry trajectories, in the lower portion of the arc the treatment couch introduced a non-negligible source of attenuation to the current signal, and has been removed from the presented data. Due to differences in the start of the electrometer current recording and the radiation delivery, the gantry angles indicated are approximate.

The current measurements for a static gantry angle and couch position indicate the stability of the linear accelerator output. This inherent output variability is expected to be consistent for the plans involving dynamic motion of the couch and/or gantry. For the deliveries involving gantry rotation, the gravitational sag of the gantry can also impact the current measurements.

To assess the worst case scenario for the positional accuracy, the only non-negligible effect on the current measurements was assumed to be due to the inverse square law. The average of the minimum and maximum recorded ionization chamber currents was assumed to correspond to the coincidence of the ionization chamber with treatment isocenter. The difference between the minimum or maximum recorded current and this average would then indicate the greatest deviation of the couch from its programmed position. Using the inverse square law, the difference in current was translated into an approximate measurement of distance. For the case of static couch and gantry position during radiation delivery, the influence of dose rate fluctuations or measurement noise can be assessed and translated into an uncertainty estimate for

the other measurements. The maximum current deviations observed correspond to ±0.04 cm, ±0.2 cm, and ±0.2 cm positional deviations of the treatment couch from the programmed isocenter for the stationary couch/stationary gantry, stationary couch/rotating gantry, and synchronous couch and gantry motion, respectively.

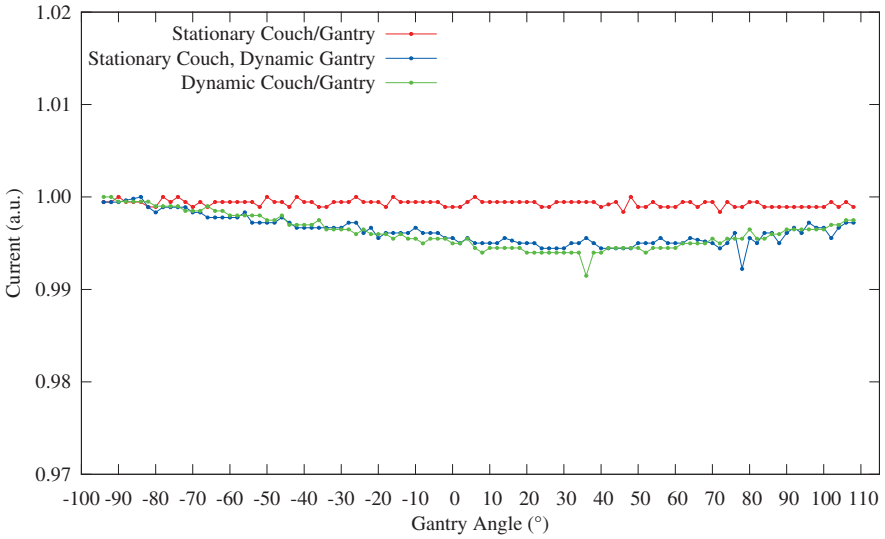

Figure 4–12: Ionization chamber current measurements taken as a function of linear accelerator gantry rotation angle. An ionization chamber was placed in a cylindrical phantom at isocenter, and radiation was delivered with programmed trajectories on the TrueBeam STx linear accelerator for static couch/gantry position, dynamic gantry rotation (analogous to VMAT treatment), and dynamic couch and gantry motion (analogous to the proposed VIRA treatment technique). The gantry angles indicated are approximate due to nonsimultaneous start of the electrometer recording and radiation delivery.

CHAPTER 5
Discussion

5.1 Dosimetric Leaf Gap, Leaf Transmission

5.1.1 Dosimetric Leaf Gap

The use of only two data points to characterize the linear regression that defines the DLG resulted in a difference of 1.3±0.8% compared to the DLG obtained using measurements for all seven sliding gaps. This corresponds to a clinically negligible measurement difference on the order of 0.02 mm. These data suggest that with a well characterized dosimetry system in which ionization chamber and electrometer stability have been thoroughly established, a two-measurement estimate of DLG has sufficient clinical accuracy.

The DLG was characterized for its dependence on SSD under 24 different measurement conditions, varying the beam energy, ionization chamber, measurement depth, and MLC model. Of these 24 datasets, 15 yielded a statistically significant dependence on SSD following corrections for geometric projection, however, this dependence is clinically insignificant based on the results of the previously mentioned studies [22, 23, 24]. The average standard deviation of the DLG estimates for each geometrically-corrected dataset was 1.31±0.09%, comparable to the standard deviation of the repeatability measurements (1.03%), suggesting a negligible effect from varying the SSD for the geometrically-corrected DLG estimates.

The DLG estimates obtained using the PTW31010 ionization chamber were greater than the estimates obtained with the large volume chambers for both depths at 6 MV, and for 5 cm depth at 18 MV. A polarity effect was investigated as a possible cause, as a leakage current would affect the charge more substantially when measured with a small volume chamber due to the lessened magnitude. A negative offset applied to the charge for each sliding gap measurement would not affect the quality of the linear regression fit, but would cause an increase of the DLG if measured with a positive electrometer polarity. However, the magnitude of the polarity effect was observed to be similar for each ionization chamber, and unable to explain the deviation in the DLG measurements. Despite also featuring a smaller collecting volume than the large volume chambers, the NE2577 chamber (collecting volume: 0.2 cm^3) did not exhibit the same offset of the DLG measurements as the PTW31010 chamber (collecting volume: 0.125 cm^3).

The average absolute difference between DLG measurements taken the same distance from the linac source but at different measurement depths was 0.03±0.02 mm, with a maximum difference of 0.08 mm. This difference is not clinically important. The degree of ion recombination effects is dependent on the dose per linac pulse, which is affected by the depth of measurement, but the correction for this effect is minimal [45].

The differences observed for the same MLC at different energies are expected; a higher energy results in a more penetrating beam, and leads to increased leakage through the rounded leaf ends, causing an increase to the DLG. This behaviour is consistent with other published results [46]. Differing characteristics between the

MLC models, specifically leaf thickness and radius of curvature of the rounded leaf ends would affect the measurement, and the DLG values are qualitatively consistent with the expected behaviour. The increased radius of curvature and leaf thickness in the HD120 MLC will cause a decrease in the transmission through the rounded leaf ends, resulting in a smaller DLG compared to the Millennium MLC.

5.1.2 Leaf Transmission

The leaf transmission measurements were observed to decrease, on average, monotonically with increasing SSD, by 0.09±0.02% over the SSD range investigated. This dependence corresponds to a dose difference decrease on the order of 1%, though this was also shown to be dependent on the MLC-defined field size [47]. Comparing LT at different measurement depths yielded an offset for the 6 MV data that was not observed with the LT measurements at 18 MV.

Possible explanations for these dependencies may involve the differences in the beam characteristics for an open field compared to the transmitted field through the MLC. One factor that may influence the transmission is the relative linear accelerator head scatter for the open field compared to the transmitted field. Interactions of the transmitted field with the MLC may also result in a different effective focal spot, causing inequal inverse square law effects compared to the open field.

The dependence on depth of measurement observed for the 6 MV measurements may be attributed to hardening of the energy spectrum of the transmitted photons. The deeper penetration into the water-equivalent phantom would result in an increase of the charge measured at 10 cm relative to 5 cm, in qualitative agreement with the LT measurements. As the LT measurements at 18 MV do not reflect this depth

dependence, further investigation into the energy spectrum of the transmission beam is required to corroborate this explanation. An additional factor for the dependence on measurement depth may be variations in the experimental conditions, as the measurements at one depth were taken during a different period than the other.

5.2 Dynamic IMRT Verification

5.2.1 Ionization Chamber Measurements

The relative agreement for eight of the eleven clinical dynamic IMRT verification plans showed a consistent dependence on SSD. On average, the relative agreement decreased by 1.5±0.3% between 85 cm SSD and 135 cm SSD. However, as indicated in Fig. 4–8, the subfields which comprise the total treatment plan featured both positive and negative dependencies on SSD. Though the aperture defined by MLC leaves may vary in width across the treatment field, the modulation factor defined at a point was assumed to approximate the degree of the overall field modulation.

Treatment plans generated in Eclipse are not initially guaranteed to adhere to the mechanical restrictions of the MLC carriage, which can define a maximum field size of 14.5 cm. When the final treatment plan or a verification plan is generated, the Eclipse TPS divides these fields into split fields to make delivery possible. A single measurement point may be entirely occluded by the collimator jaws for one of the split fields, resulting in a low modulation factor and no substantial contribution to the cumulative dose, but may feature a strong dependence on SSD. These conditions were filtered from the individual field relative agreement dependence as a function of SSD through the specification of a minimum dose threshold of 10% of the cumulative dose at each SSD for a given field. Following weighting of the relative agreement from

each field for its contribution to the cumulative dose at each SSD, 32 of the remaining 39 fields meeting these criteria featured a negative dependence on SSD.

In the literature, the dose difference was observed to be dependent on the leaf transmission estimate entered in Eclipse, while also depending on the size of the aperture defined by the MLC leaves [47]. The bias observed in Fig. 4–9 towards a negative dependence on SSD may be partially attributed to this effect, especially for fields with a low modulation factor and in accordance with the LT dependence on SSD reported previously.

5.2.2 Radiochromic Film Measurements

Radiochromic film measurements of the dynamic IMRT verification plans were performed to corroborate the results obtained with ionization chambers for the entire field rather than for a single point of measurement. When calculating the relative agreement between the film dose measurement and Eclipse dose calculations and comparing the results at 85 cm SSD and 135 cm SSD, it was observed that selecting an arbitrary region of interest was inadequate due to poor low dose radiochromic film precision, which has been known to be impacted by pixel-to-pixel noise [33]. The increasing error bars at low doses indicate the inconsistency in the data. Binning the pixels based on dose allowed the low dose inaccuracies to be isolated, while maintaining the region of interest comparison to mitigate the influence of registration errors (misalignment of dose gradients).

Though the abscissa in Fig. 4–10 is labeled as dose, this refers only to the dose at 135 cm SSD. The regions delineated at 85 cm SSD feature the same projected portion of the radiation beam from the contours defined at 135 cm SSD. Qualitatively, similar

behaviour is observed for both films in the binned regions. For dose bins greater than 0.5 Gy, the average difference in the measurements at each SSD is within ±2%, with an overestimation of the relative agreement at 85 cm SSD compared to 135 cm SSD beyond the 1.0 Gy bin of 0.5±0.4%.

Due to the differences in each clinical plan, particularly treatment site, the maximum dose delivered is not consistent. Therefore, the number of samples in each dose bin for the comparison in Fig. 4–11 decreases with increased dose. The average in the final dose bin is calculated from the data of three treatment plans.

5.3 Positional Accuracy

The three deliveries used to assess the positional accuracy of the TrueBeam patient couch are analogous to conventional IMRT or 3DCRT treatment (static gantry and couch), VMAT treatment (dynamic gantry, static couch), and the proposed VIRA treatment (dynamic gantry and couch). In the worst case scenario, assuming that the inverse square law effect is solely responsible for deviations in the measured current, the positional accuracy for treatments involving couch and/or gantry motion was estimated. The calculated positional deviation for the static gantry and couch plan indicates the standard error of the measurement. The deviation was calculated from the minimum and maximum current reading obtained during the measurement while assuming that their average value corresponded to measurement at isocenter. The calculated positional accuracy for both the VMAT analogue and the VIRA analogue was ±0.2 cm. The systematic deviation of the current measurement for both these trajectories in time may indicate that the position of the ionization chamber did not precisely coincide with the treatment plan isocenter rather than a positional

instability of the treatment couch. The addition of dynamic couch trajectories in the VIRA-analogue treatment maintained the positional accuracy expected of the VMAT-analogue treatment.

CHAPTER 6
Conclusion

The dependence of the Varian Eclipse treatment planning system was assessed as a function of SSD, through the verification of dynamic MLC IMRT treatment plan delivery and open field measurements, and investigation of the dosimetric leaf gap and leaf transmission. The average dependence observed with the dynamic IMRT verification was a decrease in the percentage agreement of Eclipse dose relative to ionization chamber measurement of 1.5±0.3% over the SSD range investigated. Gafchromic EBT3 film measurements were consistent with ionization chamber results, though noise in the film data at low doses resulted in large uncertainties. DLG was found to be independent of SSD, following corrections for geometric projection. The AAA dose calculations for modulated fields assume the measurement of the DLG under certain reference conditions, so as long as a medical physicist is cognizant of the geometric projection when measuring DLG during beam commissioning, this dependence is irrelevant. Leaf transmission decreased on average by 0.09±0.02% over the SSD range investigated. According to the literature, this corresponds to a dose difference on the order of 1%, but is dependent on the MLC-defined fields. The LT dependence on SSD is in agreement with the SSD-dependence indicated by the dynamic IMRT verification results. Investigation into the individual field dependence on SSD as a function of modulation factor illustrated the bias towards a negative dependence on SSD, which may be partially attributed to the LT dependence.

The positional accuracy of the Varian TrueBeam treatment couch was verified through radiation delivery for a dynamic couch trajectory as the real-time current was measured by an ionization chamber in a cylindrical phantom. Under the assumption that inverse square law effects are responsible for any deviation in the measured current, the same deviation of 0.2 cm was observed relative to the treatment isocenter for both the rotation gantry/stationary couch plan and the synchronous couch and gantry rotation plan, indicating the suitability of incorporating dynamic couch trajectories into VMAT treatments.

Secondary investigations explored the dependence of DLG on a variety of other factors, including depth of measurement, energy, ionization chamber, MLC model, dose rate, and the required number of sliding gap measurements to obtain an accurate DLG estimate. No clinically relevant dependence was observed on depth or dose rate, and only the PTW31010 ionization chamber yielded inconsistent results compared to the large volume chambers (though remaining a clinically irrelevant difference). The energy dependence and MLC model dependencies are consistent with results in the literature and the expected behaviour. For an accurate estimation of the DLG, only two data points, a 2 mm sliding gap and a 20 mm sliding gap, are required. The dependence of LT on depth of measurement, energy, ionization chamber, MLC model and dose rate was also examined. Different LT results were obtained for the small volume chambers (NE2577, PTW31010) compared to the large volume chambers (NE2571, ExradinA12), and a dependence on depth was observed for measurements at 6 MV, with no significant dependence at 18 MV. These results require further

investigation to ascertain their source, but it is speculated that the energy spectrum and scatter characteristics of the transmitted field are contributing factors.

The suitability of Varian Eclipse dose calculations using AAA for the implementation of dynamic couch trajectories in conjunction with VMAT optimization is best assessed by the overall dependency indicated by the dynamic IMRT ionization chamber measurements. The average dependence observed was 1.5±0.3% over the SSD range of 85 cm to 135 cm, with a difference of less than 1% relative to clinical reference conditions (100 cm SSD), indicating the necessary dosimetric accuracy for treatment plan optimization. The positional accuracy of the Varian TrueBeam couch was likewise demonstrated for dynamic couch trajectories, with ionization chamber current measurements indicating delivery accuracy that parallels the achievable accuracy in VMAT treatment.

6.1 Future Work

The results presented in this thesis indicate the suitability of dose calculations in Varian Eclipse in the context of dynamic couch trajectories. The next step towards the implementation of VIRA involves interfacing with the Eclipse Algorithm Application Programming Interface (API) for RapidArc optimization to define variable treatment couch positions corresponding to dynamic trajectories. Validation of this treatment would require delivery of plans with dynamic trajectories to a phantom on the TrueBeam, and comparing film and ionization chamber measurements to the calculated dose distributions in Eclipse.

REFERENCES

[1] J. V. Dyk, *Modern Technology of Radiation Oncology: A Compendium for Medical Physicists and Radiation Oncologists*, vol. 1. Medical Physics Pub., 1999.

[2] N. Massager, J. Lorenzoni, D. Devriendt, and M. Levivier, "Radiosurgery for Trigeminal Neuralgia," *Prog Neurol Surg*, vol. 20, pp. 235–243, 2007.

[3] M. Yamamoto, M. Jimbo, M. Hara, I. Saito, and K. Mori, "Gamma knife radiosurgery for arteriovenous malformations: long-term follow-up results focusing on complications occuring more than 5 years after irradiation," *Neurosurgery*, vol. 38, no. 5, pp. 906–914, 1996.

[4] American Medical Association, *Physician Characteristics & Distribution 2013*. American Medical Association, 2008.

[5] J. Van Dyk, *Modern Technology of Radiation Oncology: A Compendium for Medical Physicists and Radiation Oncologists*, vol. 2. Medical Physics Pub., 2005.

[6] C. Yu and G. Tang, "Intensity-modulated arc therapy: principles, technologies and clinical implementation," *Physics in Medicine and Biology*, vol. 56, pp. R31–R54, 2011.

[7] D. A. Palma, W. F. A. R. Verbakel, K. Otto, and S. Senan, "New developments in arc radiation therapy: A review," *Cancer Treatment Reviews*, vol. 36, pp. 393–399, August 2010.

[8] R. D. Timmerman, "An Overview of Hypofractionation and Introduction to This Issue of Seminars in Radiation Oncology," *Seminars in Radiation Oncology*, vol. 18, pp. 215–222, October 2008.

[9] S. H. Benedict *et al.*, "Stereotactic body radiation therapy: The report of AAPM Task Group 101," *Medical Physics*, vol. 37, pp. 4078–4101, August 2010.

[10] E. B. Podgorsak, A. Olivier, M. Pla, P.-Y. Lefebvre, and J. Hazel, "Dynamic stereotactic radiosurgery," *International Journal of Radiation Oncology, Biology and Physics*, vol. 14, no. 1, pp. 115–226, 1988.

[11] S. F. Shaitelman, L. H. Kim, D. Yan, A. A. Martinez, F. A. Vicini, and I. S. Grills, "Continuous arc rotation of the couch therapy for the delivery of accelerated partial breast irradiation: a treatment planning analysis," *International Journal of Radiation Oncology, Biology and Physics*, vol. 80, no. 3, pp. 771–778, 2011.

[12] C. C. Popescu, W. A. Beckham, V. V. Patenaude, I. A. Olivotto, and M. T. Vlachaki, "Simultaneous couch and gantry dynamic arc rotation (CG-Darc) in the treatment of breast cancer with accelerated partial breast irradiation (APBI): a feasibility study," *Journal of Applied Clinical Medical Physics*, vol. 14, no. 1, pp. 161–175, 2012.

[13] Y. Yang, P. Zhang, L. Happersett, J. Xiong, J. Yang, M. Chan, K. Beal, G. Mageras, and M. Hunt, "Choreographing couch and collimator in volumetric modulated arc therapy," *International Journal of Radiation Oncology, Biology and Physics*, vol. 80, no. 4, pp. 1238–1247, 2011.

[14] J. Van Dyk, J. M. Galvin, G. P. Glasgow, and E. B. Podgorsak, *AAPM Report No. 17: The Physical Aspects of Total and Half Body Photon Irradiation.* American Institute of Physics, 1986.

[15] I. Buzurovic, Y. Yu, M. Werner-Wasik, T. Biswas, P. R. Anne, A. P. Dicker, and T. K. Podder, "Implementation and experimental results of 4D tumor tracking using robotic couch," *Medical Physics*, vol. 39, pp. 6957–6967, November 2012.

[16] A. Van Esch, L. Tillikainen, J. Pyykkonen, M. Tenhunen, H. Helminen, S. Siljamaki, J. Alakuijala, M. Paiusco, M. Iori, and D. P. Huyskens, "Testing of the analytical anisotropic algorithm for photon dose calculation," *Medical Physics*, vol. 33, pp. 4130–4148, 2006.

[17] A. Fogliata, G. Nicolini, E. Vanetti, A. Clivio, and L. Cozzi, "Dosimetric validation of the anisotropic analytical algorithm for photon dose calculation: fundamental characterization in water," *Physics in Medicine and Biology*, vol. 51, pp. 1421–1439, 2006.

[18] M. W. K. Kan, L. H. T. Leung, R. W. K. So, and P. K. N. Yu, "Experimental verification of the Acuros XB and AAA dose calculation adjacent to heterogeneous media for IMRT and RapidArc of nasopharyngeal carcinoma," *Medical Physics*, vol. 40, pp. 031714–1, 2013.

[19] E. Sterpin, M. Tomsej, B. De Smedt, N. Reynaert, and S. Vynckier, "Monte Carlo evaluation of the AAA treatment planning algorithm in a heterogeneous multilayer phantom and IMRT clinical treatments for an Elekta SL25 linear accelerator," *Medical Physics*, vol. 34, pp. 1665–1677, 2007.

[20] A. Hussain, E. Villareal-Barajas, D. Brown, and P. Dunscombe, "Validation of the Eclipse AAA algorithm at extended SSD," *Journal of Applied Clinical Medical Physics*, vol. 11, pp. 90–100, 2010.

[21] G. A. Ezzell, J. M. Galvin, D. Low, J. R. Palta, I. Rosen, M. B. Sharpe, P. Xia, Y. Xiao, L. Xing, and C. X. Yu, "Guidance document on delivery, treatment planning, and clinical implementation of IMRT: Report of the IMRT subcommittee of the AAPM radiation therapy committee," *Medical Physics*, vol. 30, pp. 2089–2115, August 2003.

[22] J. H. Kung and G. T. Y. Chen, "Intensity modulated radiotherapy dose delivery error from radiation field offset inaccuracy," *Medical Physics*, vol. 27, pp. 1617–1622, 2000.

[23] M. R. Arnfield, K. Otto, V. R. Aroumougame, and R. D. Alkins, "The use of film dosimetry of the penumbra region to improve the accuracy of intensity modulated radiotherapy," *Medical Physics*, vol. 32, pp. 12–18, January 2005.

[24] T. LoSasso, C.-S. Chui, and C. C. Ling, "Physical and dosimetric aspects of a multileaf collimator system used in the dynamic mode for implementing intensity modulated radiotherapy," *Medical Physics*, vol. 25, pp. 1919–1927, October 1998.

[25] K. C. Younge, M. M. Matuszak, J. M. Moran, D. L. McShan, B. A. Fraass, and D. A. Roberts, "Penalization of aperture complexity in inversely planned volumetric modulated arc therapy," *Medical Physics*, vol. 39, pp. 7160–7170, November 2012.

[26] M. S. Huq, I. J. Das, T. Steinberg, and J. M. Galvin, "A dosimetric comparison of various multileaf collimators," *Physics in Medicine and Biology*, vol. 47, pp. N159–N170, June 2002.

[27] J.-W. Lee, K.-S. Choi, S. Hong, Y.-L. Kim, J.-B. Chung, D.-H. Lee, B.-Y. Choe, H.-S. Jang, and T.-S. Suh, "Effects of static dosimetric leaf gap on MLC-based small-beam dose distribution for intensity-modulated radiosurgery," *Journal of Applied Clinical Medical Physics*, vol. 8, pp. 54–64, Fall 2007.

[28] K. N. Kielar, E. Mok, A. Hsu, L. Wang, and G. Luxton, "Verification of dosimetric accuracy on the TrueBeam STx: Rounded leaf effect of the high definition MLC," *Medical Physics*, vol. 39, pp. 6360–6371, October 2012.

[29] T. Kron, A. Clivio, E. Vanetti, G. Nicolini, J. Cramb, P. Lonski, L. Cozzi, and A. Fogliata, "Small field segments surrounded by large areas only shielded by a multileaf collimator: Comparison of experiments and dose calculation," *Medical Physics*, vol. 39, pp. 7480–7489, December 2012.

[30] N. Hardcastle, P. Metcalfe, A. Ceylan, and M. J. Williams, "Multileaf collimator end effect leakage: implications for wide field IMRT," *Physics in Medicine and Biology*, vol. 52, pp. N493–N504, October 2011.

[31] Varian Medical Systems, "Eclipse 10 Inverse Planning Administration and Physics, Rev. 6.1.1," 2011.

[32] G. T. Betzel, B. Y. Yi, Y. Niu, and C. X. Yu, "Is RapidArc more susceptible to delivery uncertainties than dynamic IMRT?," *Medical Physics*, vol. 39, pp. 5882–5890, October 2012.

[33] D. A. Low, J. M. Moran, J. F. Dempsey, L. Dong, and M. Oldham, "Dosimetry tools and techniques for IMRT," *Medical Physics*, vol. 38, pp. 1313–1338, March 2011.

[34] V. Feygelman and B. E. Nelms, "Dose Verification in IMRT and VMAT," *AIP Conference Proceedings*, vol. 1345, no. 145, 2011.

[35] S. Steciw, S. Rathee, and B. Warkentin, "Modulation factors calculated with an EPID-derived MLC fluence model to streamline IMRT/VMAT second checks," *Journal of Applied Clinical Medical Physics*, pp. 62–81, 2012.

[36] E. B. Podgorsak, *Radiation Oncology Physics: A Handbook for Teachers and Students*. Vienna, Austria: IAEA, 2005.

[37] P. R. Almond, P. J. Biggs, B. M. Coursey, W. F. Hanson, M. S. Huq, R. Nath, and D. W. O. Rogers, "AAPM's TG-51 protocol for clinical reference dosimetry

of high-energy photon and electron beams," *Medical Physics*, vol. 26, pp. 1847–1870, September 1999.

[38] J. Seuntjens and H. Bouchard, "Ionization chamber-based reference dosimetry of intensity modulated radiation beams," *Medical Physics*, vol. 31, no. 9, pp. 2454–2465, 2004.

[39] M. Williams and P. Metcalfe, "Radiochromic Film Dosimetry and its Applications in Radiotherapy," *AIP Conference Proceedings*, vol. 1345, no. 75, 2011.

[40] D. Lewis, A. Micke, and X. Yu, "An efficient protocol for radiochromic film dosimetry combining calibration and measurement in a single scan," *Medical Physics*, vol. 39, pp. 6339–6350, October 2012.

[41] W. Crijns, F. Maes, U. A. van der Heide, and F. Van den Heuvel, "Calibrating page-sized Gafchromic EBT3 films," *Medical Physics*, vol. 40, p. 012102, January 2013.

[42] S. Devic, N. Tomic, C. G. Soares, and E. B. Podgorsak, "Optimizing the dynamic range extension of a radiochromic film dosimetry system," *Medical Physics*, vol. 36, pp. 429–437, February 2009.

[43] A. Micke, D. F. Lewis, and X. Yu, "Multichannel film dosimetry with nonuniformity correction," *Medical Physics*, vol. 38, pp. 2523–2534, May 2011.

[44] R. R. Mayer, F. Ma, Y. Chen, R. I. Miller, A. Bellard, J. McDonough, and J. J. Connell, "Enhanced dosimetry procedures and assessment for EBT2 radiochromic film," *Medical Physics*, vol. 39, pp. 2147–2155, April 2012.

[45] M. R. McEwen, "Measurement of ionization chamber absorbed dose kQ factors in megavoltage photon beams," *Medical Physics*, vol. 37, no. 5, pp. 2179–2193, 2010.

[46] Z. Chang, Q. Wu, J. Adamson, L. Ren, J. Bowsher, H. Yan, A. Thomas, and Y. F.-F, "Commissioning and dosimetric characteristics of TrueBeam system: Composite data of three TrueBeam machines," *Medical Physics*, vol. 39, no. 11, pp. 6981–7018, 2012.

[47] E. Wasbö and H. Valen, "Dosimetric discrepancies caused by differing MLC parameters for dynamic IMRT," *Physics in Medicine and Biology*, vol. 53, no. 2, pp. 405–415, 2008.

LIST OF ABBREVIATIONS

AAA: Analytical Anisotropic Algorithm

AAPM: American Association of Physicists in Medicine

CPE: Charged Particle Equilibrium

DLG: Dosimetric Leaf Gap

EAAPI: Eclipse Algorithm Application Programming Interface

XML: Extensible Markup Language

IMRT: Intensity Modulated Radiotherapy

LT: Leaf Transmission

MF: Modulation Factor

MLC: Multi-Leaf Collimator

QA: Quality Assurance

SAD: Source-to-Axis Distance

SSD: Source-to-Surface Distance

SBRT: Stereotactic Body Radiation Therapy

SRS: Stereotactic Radiosurgery

VIRA: Virtual Isocenter RapidArc

VMAT: Volumetric Modulated Arc Therapy